iScience

CellPress
OPEN ACCESS

Article

Mitochondrial glycerol 3-phosphate dehydrogenase deficiency exacerbates lipotoxic cardiomyopathy

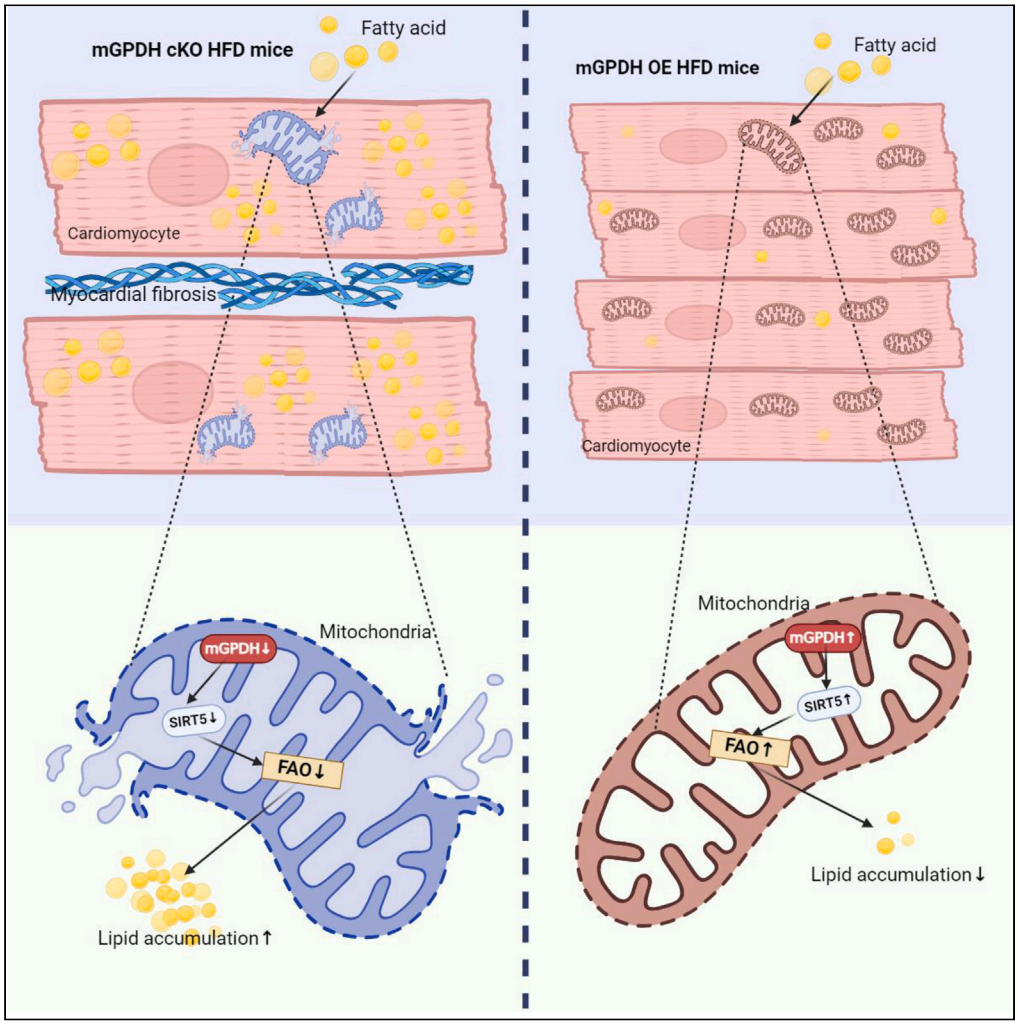

Hua Qu, Xiufei Liu, Jiaran Zhu, ..., Zhiming Zhu, Yi Zheng, Hongting Zheng

quhuahua120@163.com (H.Q.)
cecilia.zy@163.com (Y.Z.)
fnf7703@hotmail.com (H.Z.)

Highlights

Cardiac-specific deletion of mGPDH promotes HFD induced lipotoxic cardiomyopathy

mGPDH deletion inhibits SIRT5 which in turn hypersuccinylates majority FAO enzymes

Manipulating SIRT5 abolishes the effects of mGPDH modulations on cardiac functions

mGPDH restoration improves lipid deposition and cardiomyopathy in obese mice

Qu et al., iScience 27, 109796
June 21, 2024
https://doi.org/10.1016/j.isci.2024.109796

iScience

CellPress
OPEN ACCESS

Article

Mitochondrial glycerol 3-phosphate dehydrogenase deficiency exacerbates lipotoxic cardiomyopathy

Hua Qu,[1,8,*] Xiufei Liu,[1,8] Jiaran Zhu,[1,8] Niexia He,[2,8] Qingshan He,[1,8] Linlin Zhang,[1] Yuren Wang,[1] Xiaoli Gong,[1] Xin Xiong,[1] Jinbo Liu,[3] Chuan Wang,[3] Gangyi Yang,[4] Qingwu Yang,[5] Gang Luo,[6] Zhiming Zhu,[7] Yi Zheng,[1,*] and Hongting Zheng[1,9,*]

SUMMARY

Metabolic diseases such as obesity and diabetes induce lipotoxic cardiomyopathy, which is characterized by myocardial lipid accumulation, dysfunction, hypertrophy, fibrosis and mitochondrial dysfunction. Here, we identify that mitochondrial glycerol 3-phosphate dehydrogenase (mGPDH) is a pivotal regulator of cardiac fatty acid metabolism and function in the setting of lipotoxic cardiomyopathy. Cardiomyocyte-specific deletion of mGPDH promotes high-fat diet induced cardiac dysfunction, pathological hypertrophy, myocardial fibrosis, and lipid accumulation. Mechanically, mGPDH deficiency inhibits the expression of desuccinylase SIRT5, and in turn, the hypersuccinylates majority of enzymes in the fatty acid oxidation (FAO) cycle and promotes the degradation of these enzymes. Moreover, manipulating SIRT5 abolishes the effects of mGPDH ablation or overexpression on cardiac function. Finally, restoration of mGPDH improves lipid accumulation and cardiomyopathy in both diet-induced and genetic obese mouse models. Thus, our study indicates that targeting mGPDH could be a promising strategy for lipotoxic cardiomyopathy in the context of obesity and diabetes.

INTRODUCTION

Chronic metabolic diseases, such as the dual epidemic of obesity and type 2 diabetes, are urgent public health challenges worldwide, and they can result in a specific form of cardiomyopathy termed lipotoxic cardiomyopathy.[1–3] Independently of coronary artery disease and hypertension, this form of cardiomyopathy mainly impacts myocardial structure and pump performance and is a major cause of morbidity and mortality with the rising prevalence in parallel with increases in the incidence of obesity and type 2 diabetes mellitus in developed nations.[4–6] Despite the severity and poor prognosis, there are currently no specific drugs or formal management approved for its treatment, mainly due to the pathogenic mechanisms underlying the development of the disease are not fully understood.

Mitochondrial dysfunction is considered the central event in cardiomyopathy induced by metabolic disturbance;[7] however, the exact mechanisms remain elusive. Our previous studies focused on an integral component of the mammalian respiratory chain, mitochondrial inner membrane protein glycerol 3-phosphate dehydrogenase (mGPDH, encoded by the GPD2 gene),[8] and discovered its vital role in mitochondrial function.[9] In addition, we and other groups also reported it as a regulator of both lipid and glucose metabolism in the liver.[10,11] However, the participation of mGPDH in the heart is currently unrevealed; therefore, to determine the role of mGPDH in cardiac function, and whether it contributes to the development and progression of lipotoxic cardiomyopathy is of great interest.

In this study, we provided *in vivo* and *in vitro* evidence to elucidate that the deficiency of cardiac mGPDH seen in both patients and mice with obesity and type 2 diabetes contributed to excessive lipid accumulation and cardiomyopathy. Myocardial mGPDH expression presented the clinical relevance with cardiac function in human heart tissue, and its deficiency impaired lipid regulation by modulating the SIRT5-dependent desuccinylation of fatty acid oxidation (FAO) enzymes. Moreover, rescuing the insufficient mGPDH expression in cardiomyocytes of obese mice promoted lipid metabolism and mitigated cardiomyopathy. Thus, mGPDH emerged as a potential therapeutic target for lipotoxic cardiomyopathy associated with obesity and diabetes.

[1]Department of Endocrinology, Translational Research of Diabetes Key Laboratory of Chongqing Education Commission of China, the Second Affiliated Hospital of Army Medical University, Chongqing, China
[2]Department of Ultrasound, The Second Affiliated Hospital of Army Medical University, Chongqing, China
[3]Department of Endocrinology, Qilu Hospital of Shandong University, Jinan, China
[4]Department of Endocrinology, the Second Affiliated Hospital of Chongqing Medical University, Chongqing, China
[5]Department of Neurology, the Second Affiliated Hospital of Army Medical University, Chongqing 400037, China
[6]Department of Orthopedics, the Second Affiliated Hospital of Army Medical University, Chongqing 400037, China
[7]Department of Hypertension and Endocrinology, the Third Affiliated Hospital of Army Medical University, Chongqing, China
[8]These authors contributed equally
[9]Lead contact
*Correspondence: quhuahua120@163.com (H.Q.), cecilia.zy@163.com (Y.Z.), fnf7703@hotmail.com (H.Z.)
https://doi.org/10.1016/j.isci.2024.109796

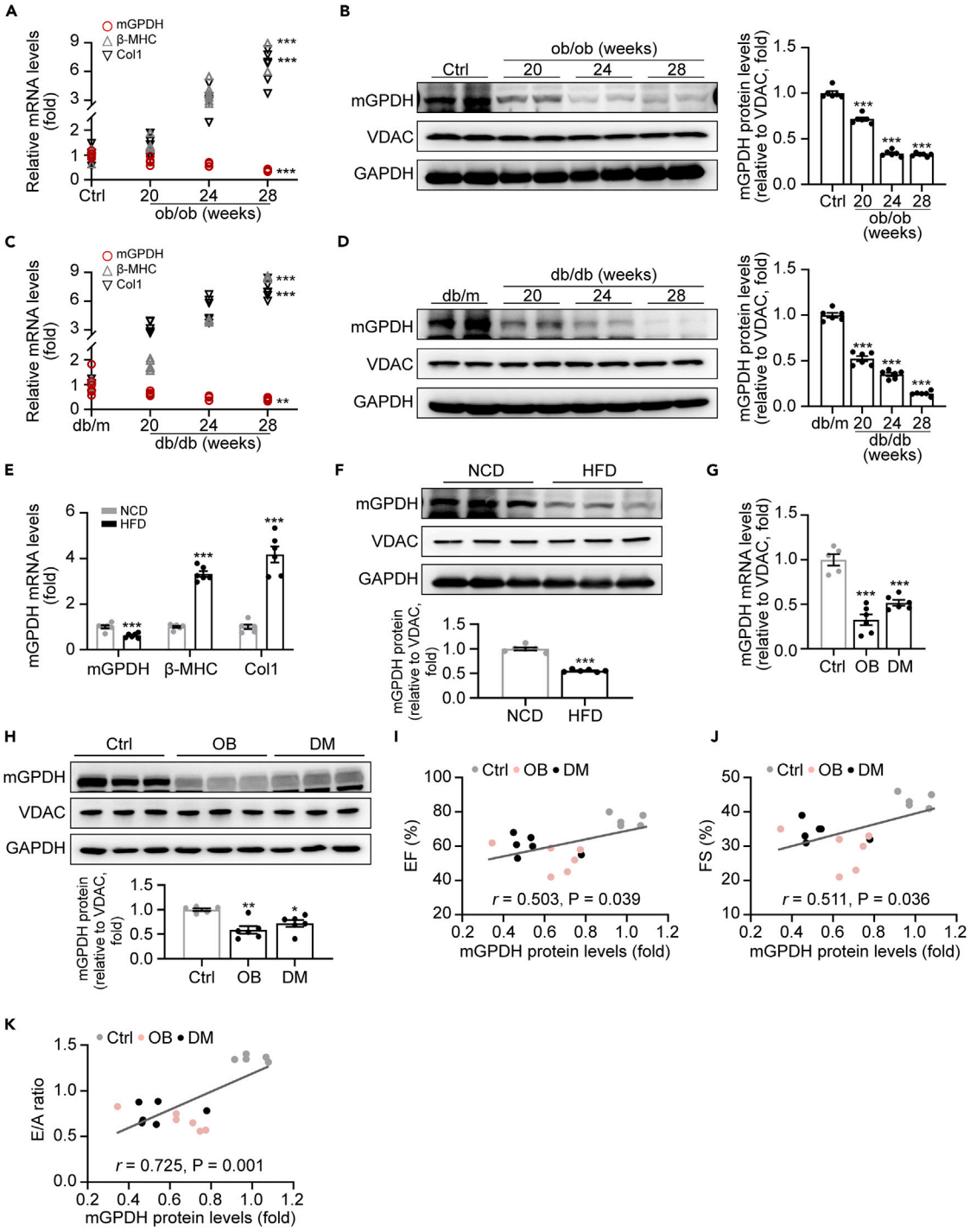

Figure 1. Cardiac mGPDH expression is reduced in patients with obese and diabetic and mouse models

(A–D) mRNA expression of mGPDH (relative to VDAC, a mitochondrial structural protein), β-myosin heavy chain (β-MHC) and collagen type 1 (Col1) in cardiac tissue from ob/ob (A), db/db (C) and their control mice at indicated weeks. Protein levels and their quantifications of mGPDH in cardiac tissue from ob/ob (B) and db/db (D) mice at indicated weeks.

(E and F) mRNA expression of mGPDH (relative to VDAC), β-MHC and Col1 in cardiac tissue from HFD-fed mice and their controls (E). Protein levels and quantifications of mGPDH in cardiac tissue from HFD-fed mice and their controls (F).

(G and H) mRNA (G) and protein (H) expressions of mGPDH in samples of the atrial appendage from patients with obese, diabetic and lean/non-diabetic controls.

Figure 1. *Continued*

(I–K) Correlation between heart mGPDH protein expression and LV ejection fractions (EF, I), fractional shortening (FS, J), or the ratio of early and late LV diastolic filling velocities (E/A ratio, K) in all subjects. $n = 6$ mice per group for A-F, n = 5–6 per group for G-K. The data are presented as the means ± S.E.M. ***$p < 0.001$ by one-way ANOVA test for A-D, G, and H, by two-tailed unpaired Student's t test for E and F.

RESULTS

Cardiac mGPDH expression is reduced in obese and diabetic mice and patients

To elucidate the role of mGPDH during the development of lipotoxic cardiomyopathy, we first analyzed its expression in cardiac tissue from mouse models of obesity and diabetes by qRT-PCR and western blot. Along with the elevated markers of cardiac hypertrophy β-myosin heavy chain (β-MHC) and fibrosis collagen type I (Col1), we found that both mGPDH mRNA and protein expressions were significantly decreased in the hearts of gene mutated ob/ob and db/db mice at 20 weeks old, and sustained decline at least to 28 weeks old (Figures 1A–1D). Consistent results were observed in obese and diabetic mice induced by high-fat diet (HFD) consumption or streptozotocin (STZ) injection, in which mGPDH expression was decreased in the hearts after 24 weeks of HFD feeding (Figures 1E and 1F), and 16 weeks after the onset of type 1 diabetes (Figures S1A and S1B), despite the reduction in STZ mice was relatively weak in contrast to the other models.

To futher confirm whether these findings are pertinent in patient, we detected mGPDH expression in myocardial samples from patients with obese and diabetic. The results showed mGPDH mRNA and protein levels were reduced in patients in contrast to lean/non-diabetic controls (Figures 1G and 1H). Interestingly, myocardial mGPDH expression elicited significant positive correlations with left ventricular (LV) ejection fraction (EF), fractional shortening (FS) and E/A ratio (ratio between early and late LV diastolic filling velocities) (Figures 1I–1K, and Table S1), which are important parameters for evaluating the cardiac function of lipotoxic cardiomyopathy. In addition, the expression of cytoplasmic glycerol 3-phosphate dehydrogenase (cGPDH, encoded by gene GPD1), another enzyme constituting the glycerol-3-phosphate shuttle with mGPDH, was not significantly changed in obese and diabetic mice and patients (Figure S2). Taken together, the simultaneous down-regulation of mGPDH expression observed in the myocardium of patients and mice indicates the potential involvement of mGPDH in lipotoxic cardiomyopathy associated with obesity and diabetes.

Cardiac-specific mGPDH deletion exacerbates cardiac injury in high-fat diet-induced cardiomyopathy

To explore the role of mGPDH deficiency in cardiac dysfunction under lipotoxic cardiomyopathy, we generated a cardiac-specific mGPDH ablation (cKO) mouse model by injecting $mGPDH^{fl/fl}$ mice with AAV9 that carries Cre recombinase under the cardiac troponin T promoter (AAV9-cTnT-Cre), and AAV9-cTnT-Cre injected $mGPDH^{wt/wt}$ mice were used as controls (Ctrl).[12,13] Then, both cKO and its control mice were induced obesity by 24 weeks of HFD consumption, a model was reported to elicit lipotoxic cardiomyopathy according to previous researches.[2,14,15] Cardiac-specific mGPDH excision of cKO mice was confirmed by qRT-PCR and immunoblotting analysis (Figures S3A and S3B). Mice with obesity showed an increased fasting plasma glucose (FPG) and body weight when compared with normal chow diet (NCD) (Figures 2A and 2B); whereas mGPDH cKO did not change FPG and body weight under both NCD and HFD conditions (Figures 2A and 2B). Echocardiography analysis revealed that the LV systolic function indices EF and FS, as well as LV diastolic function marker E/A ratio, were significantly declined in HFD-fed cKO mice in comparison with HFD-fed control littermates (Figure 2C), indicating a worsening of cardiac function induced by mGPDH deletion under HFD conditions. Moreover, HFD-fed cKO mice presented severe cardiac hypertrophy, as evidenced by increased heart weight to tibia length ratio (HW/TL) (Figure 2D), and altered expressions of myocardial hypertrophic genes, such as downregulated α-MHC, and upregulated β-MHC, atrial natriuretic peptide (ANP) and brain natriuretic peptide (BNP) (Figure 2E). Hematoxylin and eosin (H&E) staining of myocardial tissue sections showed that mGPDH cKO increased cardiac myocyte size under HFD feeding as well (Figure 2F, upper). In addition, HFD-induced cardiac fibrosis detected by Masson's Trichrome staining was significantly aggravated in cKO mice in comparison with control mice (Figure 2F, bottom). These results indicated that cardiac-specific mGPDH deficiency exacerbates cardiac dysfunction and morphological abnormalities during HFD induced lipotoxic cardiomyopathy.

mGPDH deletion promotes cardiac lipid accumulation by altering the fatty acid oxidation

Fatty acids (FAs) are the main substrates for energy generation in adult hearts, which are regulated by the processes of FA uptake and oxidation (FAO). The disruption of any of these processes can result in an imbalance of cardiac FA metabolism, leading to FA accumulation, a well-recognized pathogenesis of lipotoxic cardiomyopathy.[2,16,17] Using Oil Red O staining, we observed a significant increase of intramyocardial lipid accumulation in HFD-cKO mice compared to HFD-Ctrl mice (Figure 3A). Meanwhile, liquid chromatography/mass spectrometry (LC/MS)-based lipidomic analysis showed that long-chain FAs and triglyceride (TG) were increased in HFD-cKO mice (Figures 3B and 3C), indicating the balance of FA metabolism is disrupted in mGPDH deficient hearts. In addition, ceramides (Cer) and diacylglycerols (DAGs), the well-recognized toxic FAs were analyzed, as they were reported to mediate lipotoxic cardiomyopathy.[18–21] Our results showed that Cer(d18:1/16:0), Cer(d18:1/24:1), DAG(16:0/16:0) and DAG(18:0/18:1) were significantly higher in HFD-cKO mice (Figure S4), which validated the accumulation of toxic FAs in heart tissue. Next, we assessed which process of FA metabolism was disrupted after mGPDH deletion. By culturing isolated primary cardiomyocytes in ^{13}C-labeled palmitic acid (PA) and analyzing the concentration of labeled PA in the medium over time with LC/MS, HFD feeding did induce a significant increase in PA uptake, while it was comparable between cKO and control mice (Figure 3D). Consistently, mGPDH deficiency did not change mRNA and protein expressions of genes coding FA uptake under either condition (Figures S5A and S5B). Remarkably, we assessed FAO rate by ^{13}C-labelling assay *in vitro* and *ex vivo*,[14,22,23] and by Seahorse analysis[2,14,24] according to previous reports, and all these assays showed similar results that the FAO was significantly decreased in primary cardiomyocytes

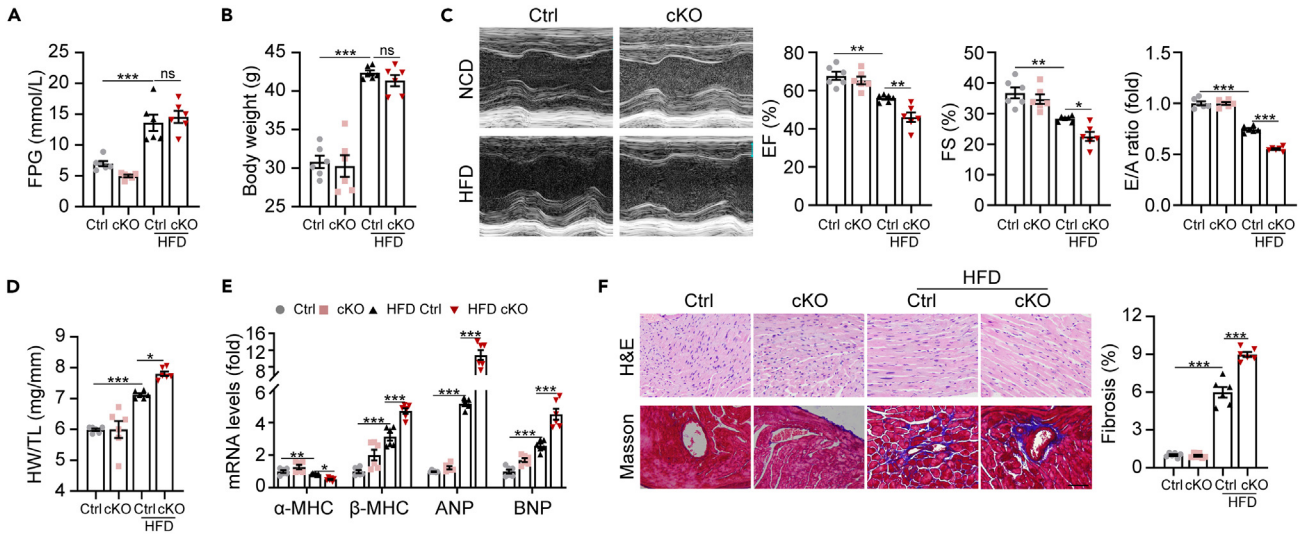

Figure 2. Cardiomyocyte-specific deletion of mGPDH exacerbates HFD-induced cardiomyopathy

Cardiomyocyte-specific mGPDH knockout mice (cKO) and its control mice (Ctrl) were fed with high-fat diet (HFD) or normal chow diet (NCD) for 24 weeks.

(A and B) Fasting glucose (FPG) levels (A) and body weight (B) of HFD- and NCD-fed mGPDH cKO and Ctrl mice.

(C) Representative echocardiographic images showing LV M-Mode traces, and LV EF, FS, and E/A ratio were calculated in HFD- and NCD-fed cKO and Ctrl mice.

(D and E) Heart weight (HW) to tibia length (TL) ratio (D) and hypertrophic gene expression (E) of HFD- and NCD-fed cKO and Ctrl mice.

(F) H&E, Masson's Trichrome staining and fibrosis quantifications in HFD- and NCD-fed cKO and Ctrl mice. Scale bar, 50 μm for F. n = 6 mice per group for A-F.

The data are presented as the means ± S.E.M. *$p < 0.05$, **$p < 0.01$, ***$p < 0.001$ by one-way ANOVA test.

and myocardium of HFD-cKO mice in comparison with HFD-Ctrl mice (Figures 3E, S5C, and S5F). In accordance, a reduced FAs-driven energy generation was obtained in mitochondria isolated from HFD-cKO mice hearts (Figure 3G). We also examined the expressions of several FAO-related enzymes such as ACADL, ACADM, ACADVL, and ECHS1,[2,14] and the results showed a markedly decrease in protein expression, but not in mRNA level in HFD-fed cKO mice comparing to HFD-Ctrl mice (Figures 3H and S5D). Additionally, the transcriptional regulators of FAO enzymes peroxisome proliferator-activated receptor α (PPARα) and PPARδ[25] were not altered either in the heart (Figure S5D). These results suggest post-translational regulation is involved in mGPDH deficiency attenuated FAO enzymes.

mGPDH deficiency suppresses cardiac fatty acid oxidation and exacerbates lipid derangement through SIRT5

Next, we questioned how mGPDH modulated FAO and cardiac function. Considering post-translational modifications (PTMs) may mediate mGPDH deletion and repress FAO-related enzymes, and nicotinamide adenine dinucleotide $(NAD)^+$-dependent histone deacetylases, sirtuins, has been widely considered as a key upstream regulator to remove these PTMs[5,26,27] and play an important role in the mechanisms involved in cardiomyopathy under obesity and diabetes,[4,5] we then measured the expression of all 7 members of sirtuins. The results showed that SIRT3 and 5 were reduced in hearts of HFD-cKO mice (Figure 4A). Thus, the participation of SIRT3 and (/or) SIRT5 in mGPDH-regulated cardiac FAO and FA accumulation were assessed. Re-introduction of SIRT5 by plasmids significantly abrogated mGPDH knockdown-induced FA overload and the reduction of FAO rate in PA-treated cardiomyocytes, while SIRT3 overexpression did not (Figures 4B and 4C). Moreover, to confirm the involvement of SIRT5 under the effect of mGPDH *in vivo*, AAV9-cTnT-SIRT5 was tail injected to induce SIRT5 in hearts of HFD-cKO and HFD-Ctrl mice (Figure S6). SIRT5 overexpression abolished mGPDH cKO induced cardiac systolic and diastolic dysfunctions, hypertrophy, fibrosis, and lipid accumulation (Figures 4D–4I), indicating that SIRT5 involves in mGPDH deletion exacerbates cardiomyopathy and cardiac lipotoxic under HFD conditions. Furthermore, we asked how mGPDH regulated SIRT5 expression? Given a unique feature of NAD^+-dependence in the sirtuins family, and our previous studies revealed an NAD^+ regulated role of mGPDH in skeletal muscle and kidney,[9,28] we evaluated the possibility that NAD^+ mediated this effect. NAD^+ levels were reduced in HFD-cKO mice (Figure S7A), and downregulating NAD^+ levels by FK866 (a specific inhibitor of the NAD^+ biosynthetic enzyme NAMPT) significantly decreased SIRT5 expression *in vivo* and *in vitro* (Figure S7B), which suggested that the deceased SIRT5 expression may related to NAD^+ reduction. This was further confirmed by that the elimination of NAD^+ by FK866 application abrogated mGPDH modulated SIRT5 expression (Figure S7C). Moreover, supply of NAD^+ precursor nicotinamide mononucleotide (NMN) successfully abrogated mGPDH knockdown-repressed SIRT5 expression in PA-treated cardiomyocytes (Figure 4J). Taken together, these findings reveal that mGPDH insufficiency accelerates obese-induced cardiac dysfunction and lipotoxicity via the inhibition of SIRT5 expression.

SIRT5 regulated the degradation of fatty acid oxidation enzymes by lysine desuccinylation

Despite belonging to the histone deacetylase family, SIRT5 was documented to possess a strong desuccinylase activity, and its deacetylase activity is weak.[27,29] Furthermore, by profiled acyl-CoA concentrations in heart tissue from mGPDH cKO mice through LC/MS, we found that

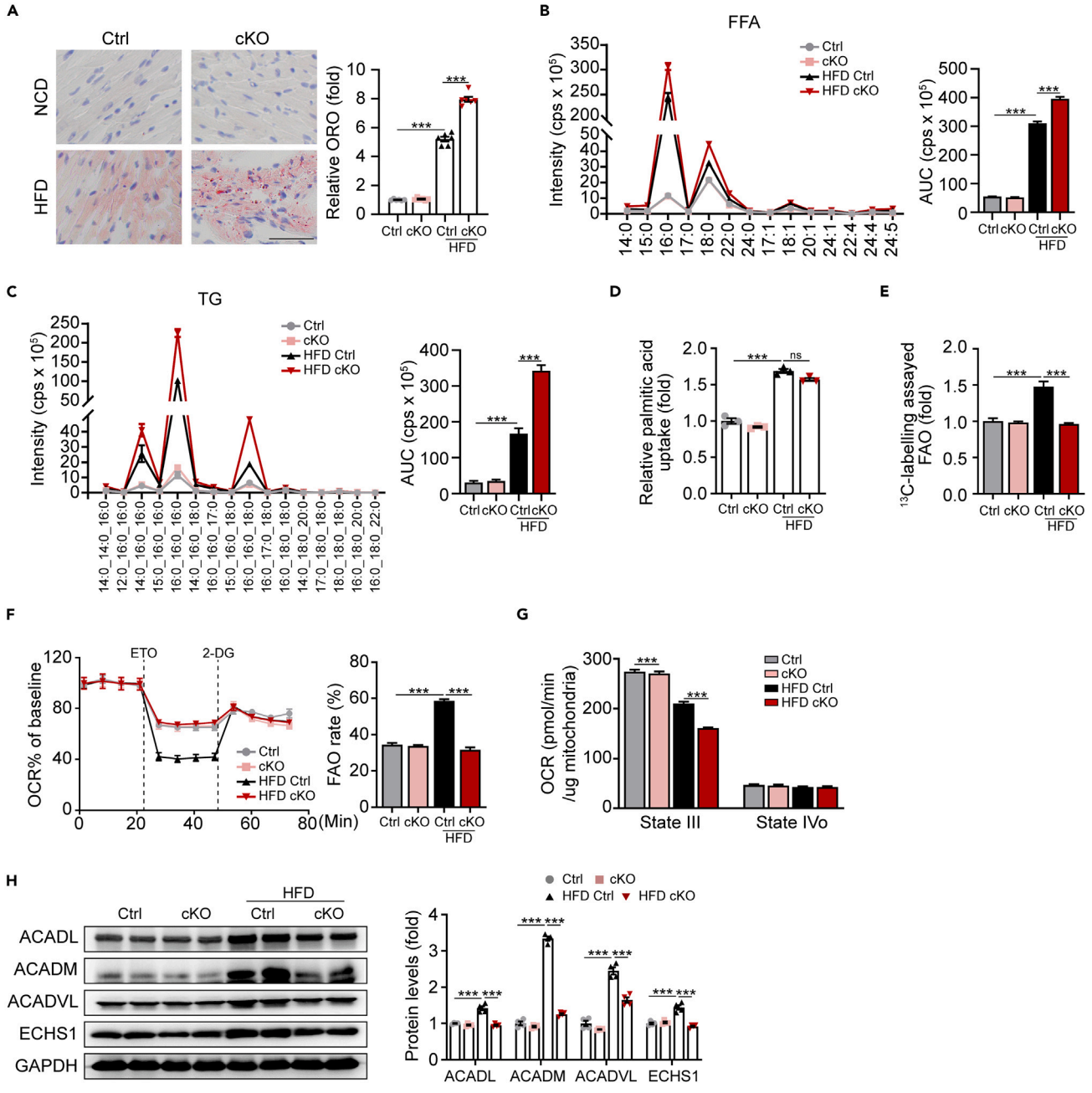

Figure 3. mGPDH deletion suppresses myocardial FAO and energetics, and promotes cardiac lipid accumulation

(A) Oil red O staining in HFD- and NCD-fed mGPDH cKO and Ctrl mice at 24 weeks after HFD feeding.

(B and C) Cardiomyocytes were isolated, and UPLC-MS/MS analysis was conducted in cardiomyocytes from different groups. Ion chromatograms and quantifications of long-chain free fatty acids (FFA, B) and triglyceride (TG, C) were shown.

(D) Cardiomyocytes were isolated from indicated mice, palmitic acid uptake were determined by ^{13}C labeling palmitic acid using the UPLC-MRM-MS method.

(E and F) Fatty acid oxidation (FAO) in cardiomyocytes from indicated mice were evaluated by the quantification of ^{13}C-palmitic acid contribution to M+2 citrate (E) and by etomoxir (ETO)-inhibitable OCR measured by Seahorse analyzer, in which FAO rate was quantified by the ratio of FAO versus total OCR (F).

(G) Mitochondria were isolated from indicated mice, and mitochondrial energetics were evaluated by palmitoyl-*l*-carnitine/malate driven respiration measured by Seahorse analyzer. State III (+ADP) and state IVo (+oligomycin).

(H) Expressions of indicated FAO proteins were detected by western blot in cardiac tissue from indicated mice. Scale bar, 50 μm for A. n = 6 mice per group for A, *n* = 3 mice per group for B-G. *n* = 4 mice per group for H. The data are presented as the means ± S.E.M. ***$p < 0.001$, ns, not significant by one-way ANOVA test.

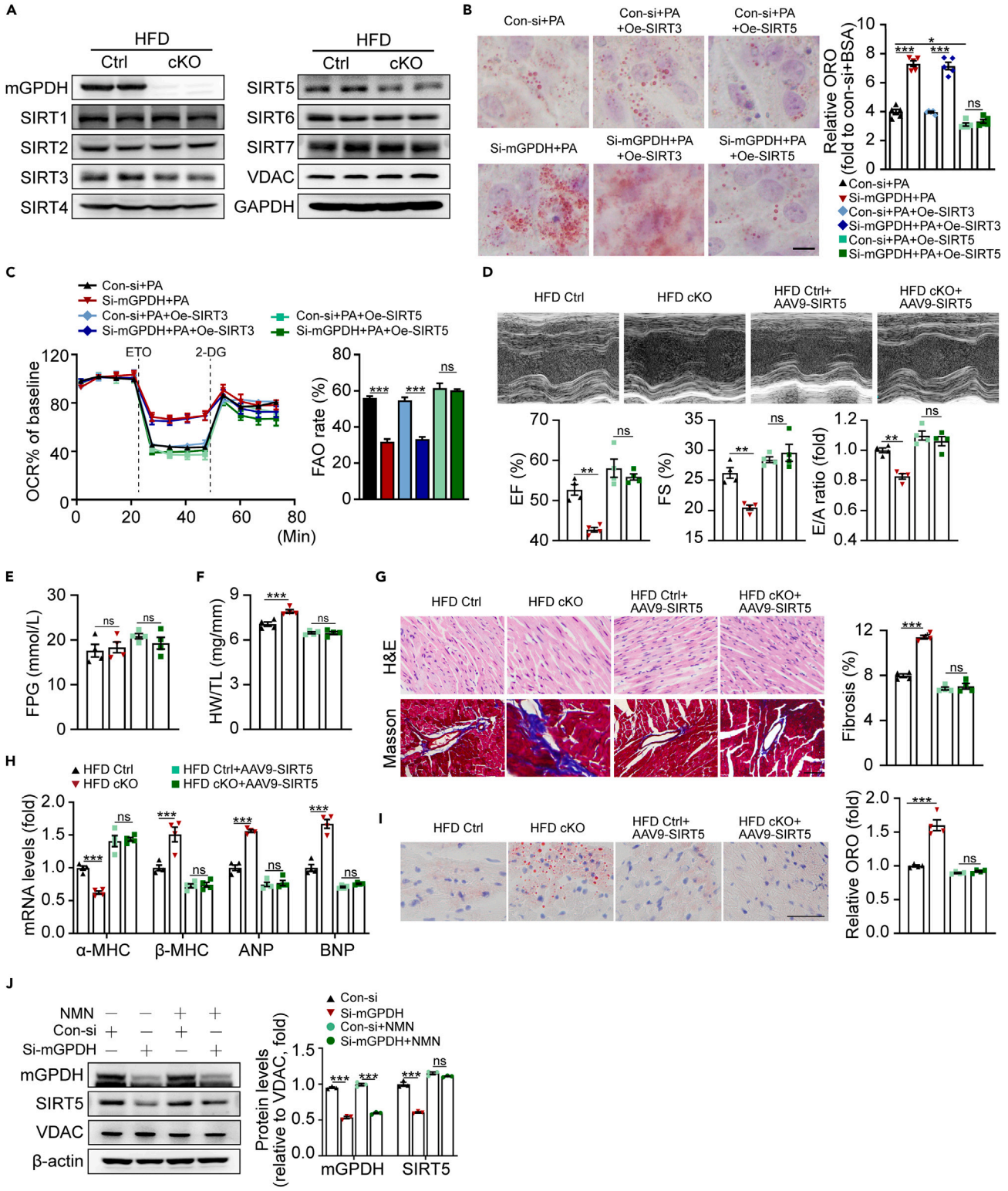

Figure 4. SIRT5 mediates mGPDH deficiency exacerbates cardiac lipid derangement and cardiomyopathy

(A) Protein expression of SIRT1-7 in heart lysates from HFD- and NCD-fed mGPDH cKO and Ctrl mice at 24 weeks after HFD feeding.

(B and C) PA-treated H9C2 cells were transfected with siRNA for mGPDH and overexpression plasmids for SIRT3 or SIRT5, lipid accumulation was assessed by Oil red O staining (B), and FAO was evaluated by etomoxir (ETO)-inhibitable OCR and FAO rate was quantified (C).

Figure 4. *Continued*

(D–I) HFD-fed cKO and Ctrl mice infected with AAV9-cTnT-SIRT5, and the representative echocardiographic images of LV M-Mode traces were shown, and LV EF, FS, and E/A ratio were calculated (D). Fasting glucose (E), HW/TL ratio (F), and hypertrophic gene expression (G) in heart from indicated groups. (H and I) H&E and Masson's Trichrome staining (H), and Oil red O staining (I) in different groups and their quantifications were shown.

(J) H9C2 cells were transfected with siRNA for mGPDH and treated with PA and NMN, expressions and quantifications of indicated proteins were shown. Scale bar, 20 μm for B; 50 μm for H and I. n = 6 per group for A, *n* = 3 for C and J, *n* = 5 for B, *n* = 4 mice per group for D–I. The data are presented as the means ± S.E.M. $*p < 0.05$, $**p < 0.01$, $***p < 0.001$, ns, not significant by one-way ANOVA test.

the predominant alterations were occurred in succinylation, when compared with other modifications (acetylation and so forth, Figure S8A). In addition, we observed the effect of SIRT5 expression alteration on it desuccinylase activity. In line with previous studies,[27,30,31] up- or down-regulated SIRT5 expression altered its desuccinylation activity *in vivo* and *in vitro* (Figure S8B). Therefore, we explored the lysine succinylation status of heart tissues in mGPDH cKO and Ctrl mice (Figure 5A). Nano LC-MS/MS analysis was performed, and results of proteomics revealed 268 lysine succinylation sites across 163 proteins that are potentially regulated by mGPDH (Fold Change >1.5 or <0.67, Figure 5B and Table S2). Of these identified sites, 77% were increased abundance in obese cKO hearts (Table S2), which suggested that hypersuccinylation was generated after mGPDH deleting. Kyoto Encyclopedia of Genes and Genome (KEGG) analysis suggested the top 3 enriched pathways among lysine-succinylated proteins including propanoate metabolism, citrate cycle, and fatty acid degradation (Figure 5C, and Table S3), and they all related to FAO. In general, there are 4 key enzymatic steps including 11 enzymes and 4 different auxiliary enzymes in FAO cycle[32] (Figure 5D). Notably, 14 enzymes in FAO cycle displayed an altered succinylation level after mGPDH deletion (13 increased and 1 decreased) under HFD feeding (Figures 5D and 5E, and Table S4). However, desuccinylation by SIRT5-overexpression in HFD-cKO heart restored most of the mGPDH deletion-induced hypersuccinylated sites of FAO enzymes (Figure 5E, and Table S4), indicating that suppressed cardiac FAO by mGPDH inhibition relates to SIRT5-mediated lysine desuccinylation.

We then examined the most evidently changed FAO enzymes, i.e., short-chain acyl-CoA dehydrogenase (SCAD, coded by ACADS) and medium-chain acyl-CoA dehydrogenase (MCAD, coded by ACADM), which were 5.4- and 4.0-fold increase in abundance of HFD-fed cKO heart. ACADS and ACADM are soluble, matrix-localized enzymes, and are well-established in the FAO cycle in humans.[32] Both of them were respectively immunoprecipitated from hearts of obese cKO and Ctrl mice, and then probed the succinylation level using an anti-succinyllysine antibody. Although deficiency of mGPDH resulted in decreased SIRT5, as well as the total abundance of ACADS and ACADM, the extent of lysine succinylation on both, were indeed greatly increased in the heart of the cKO mouse (Figure 5F). Similar results were obtained in PA-treated H9C2 cells, ACADS and ACADM were also hypersuccinylated when transfected with mGPDH-siRNA compared with control-siRNA (Figure 5G). Moreover, in mGPDH-knockdown cells, the hypersuccinylated level of ACADS was reduced after overexpressing SIRT5_WT plasmid, but not in cell transfected with kinase-dead SIRT5_H158Y (Figure 5H), suggesting mGPDH/SIRT5 induces ACADS via its lysine desuccinylation.

We next questioned how mGPDH/SIRT5 signaling induced protein level of ACADS. Figure S9 showed ACADS transcript is comparable between HFD-cKO and HFD-Ctrl heart, indicating that the mechanisms underlying might involve the regulation of ACADS protein stability. Previous studies suggested that SIRT5 can regulate protein stability by influencing ubiquitination.[33–35] To test this possibility, we treated cardiomyocytes with mGPDH siRNA and ubiquitin-proteasome inhibitor MG132 (MG). The results showed that MG abolished the reduction of ACADS protein levels seen in mGPDH knockdown cells (Figure 5I). Then, we immunoprecipitated ACADS from mGPDH-knockdown cell lysates and detected ubiquitination levels using an anti-ubiquitin antibody. The ubiquitinated level of ACADS was significantly increased after mGPDH knockdown (Figure 5J). These findings indicate that mGPDH/SIRT5 modulated ACADS protein degradation may also through the ubiquitination pathway. In addition, previous study[36] reported that autophagy-lysosome could mediate SIRT5 inhibited protein degradation as well. Therefore, this possibility was observed. mGPDH silencing reduced ACADS protein was attenuated after chloroquine treatment (Figure S10), which indicates that the autophagy pathway may also participate the effects of SIRT5 on ACADS protein.

To further elucidate which succinyllysine site of ACADS is responsible for its protein degradation, we resorted to our high-throughput screening and found that lysine residues K250 of ACADS was the only identified site which might correspond to the increased succinylated peptides. We then generated plasmids expressing HA-tagged ACADS with K-to-R mutant (mimicking the desuccinylated state) or K-to-E mutant (mimicking the negatively charged succinyllysine modification). As a result, both mutations decreased the overall succinylation levels of ACADS (Figure 5K), which confirmed that K250 is the key succinylation site on ACADS regulated by mGPDH/SIRT5. In addition, we ectopically expressed the HA-tagged ACADS_WT or mutated plasmid (ACADS_K250R or ACADS_K250E) in mGPDH silenced cardiomyocytes. As expected, the deletion of mGPDH resulted in reduced levels of ACADS in cells treated by ACADS_WT, but not in mutated plasmids (Figure 5L), indicating that the protein degradation of ACADS might be related to K250 succinylation. Furthermore, we confirmed that 2 succinylation-defective ACADS variants were less ubiquitinated than ACADS_WT (Figure 5M). Collectively, these results indicate that the K250 desuccinylation of ACADS may responsible for mGPDH/SIRT5 inhibited ACADS degradation.

Rescue of mGPDH alleviates cardiac dysfunction in high-fat diet-induced and ob/ob mice

To evaluate the effects of mGPDH rescue on lipotoxic cardiomyopathy, we injected HFD-induced and ob/ob mice with AAV9 that carries mGPDH under promoter cTnT (AA9-cTnT-mGPDH). AA9-cTnT-mGPDH exclusively increased mGPDH expression in cardiac tissue in both obese mouse models when compared with other organs such as skeletal muscle, kidney and liver (Figure S11A). Along with this, LV systolic and diastolic dysfunction including the decline of EF, FS, and E/A ratio were significantly improved in AA9-cTnT-mGPDH treated HFD mice at 8 weeks after AAV9 injection (Figure 6A). In addition, although no effects on FPG (Figure 6B), AA9-cTnT-mGPDH treatment attenuated

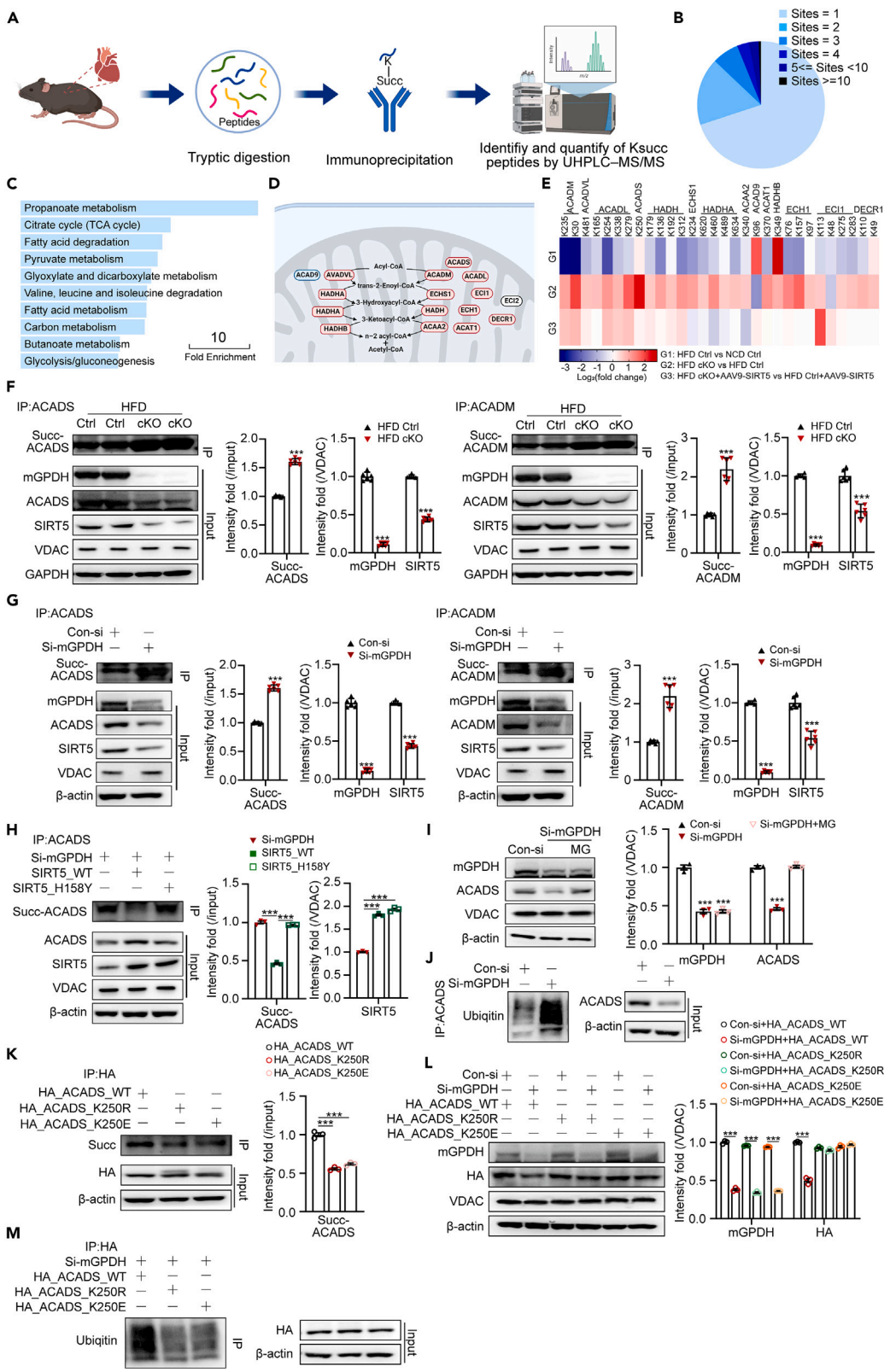
A
Peptides
Tryptic digestion
Succ
Immunoprecipitation
Identify and quantify of Ksucc peptides by UHPLC–MS/MS
B
Sites = 1
Sites = 2
Sites = 3
Sites = 4
5<= Sites <10
Sites >=10
C
Propanoate metabolism
Citrate cycle (TCA cycle)
Fatty acid degradation
Pyruvate metabolism
Glyoxylate and dicarboxylate metabolism
Valine, leucine and isoleucine degradation
Fatty acid metabolism
Carbon metabolism
Butanoate metabolism
Glycolysis/gluconeogenesis
10
Fold Enrichment
D
Acyl-CoA
trans-2-Enoyl-CoA
3-Hydroxyacyl-CoA
3-Ketoacyl-CoA
n−2 acyl-CoA
+
Acetyl-CoA
ACADS
ACADM
ACADL
ACADVL
ACAD9
HADHA
ECHS1
ECI1
ECI2
HADH
ECH1
DECR1
ACAA2
ACAT1
E
ACADM
ACADVL
ACADL
ACADS
HADH
ECHS1
HADHA
ACAD9
ACAA2
ACAT1
HADHB
ECH1
ECI1
DECR1
G1
G2
G3
G1: HFD Ctrl vs NCD Ctrl
G2: HFD cKO vs HFD Ctrl
G3: HFD cKO+AAV9-SIRT5 vs HFD Ctrl+AAV9-SIRT5
Log2(fold change)
F
IP:ACADS
HFD
Ctrl Ctrl cKO cKO
Succ-ACADS
mGPDH
ACADS
SIRT5
VDAC
GAPDH
IP
Input
HFD Ctrl
HFD cKO
Intensity fold (/input)
Intensity fold (/VDAC)
Succ-ACADS
mGPDH
SIRT5
IP:ACADM
Succ-ACADM
ACADM
G
IP:ACADS
Con-si
Si-mGPDH
β-actin
Con-si
Si-mGPDH
IP:ACADM
H
IP:ACADS
Si-mGPDH
SIRT5_WT
SIRT5_H158Y
Succ-ACADS
I
Si-mGPDH
Con-si
MG
Si-mGPDH+MG
J
IP:ACADS
Ubiqitin
K
IP:HA
HA_ACADS_WT
HA_ACADS_K250R
HA_ACADS_K250E
Succ
HA
L
Con-si+HA_ACADS_WT
Si-mGPDH+HA_ACADS_WT
Con-si+HA_ACADS_K250R
Si-mGPDH+HA_ACADS_K250R
Con-si+HA_ACADS_K250E
Si-mGPDH+HA_ACADS_K250E
M
IP:HA
Ubiqitin

Figure 5. Downregulated mGPDH/SIRT5 signaling inhibits the desuccinylation of FAO proteins and promotes ACADS degradation

(A) Schematic of experimental workflow for the identification of lysine succinylation substrates by proteomics in heart lysates.

(B) The distribution of the number of lysine succinylation site identifications per protein was shown.

(C) Top 10 terms of KEGG pathway analysis in succinylated protein targeted by mGPDH cKO under HFD condition.

(D) Schematic represents 4 steps and 15 enzymes (including 4 auxiliary enzymes) of mitochondrial FAO. 14 of them displayed an altered succinylation level after mGPDH cKO, 13 were increased (highlighted with red color) and 1 was decreased (blue). The rest one which succinylation level could not be detected was shown in white. These enzymes are showing by their gene name.

(E) Heatmap shown the changes in the levels of lysine succinylation on FAO enzymes according to our quantitative proteomics.

(F and G) Heart lysates from HFD-fed mGPDH cKO and Ctrl mice (F), and cell lysates from H9C2 cells with mGPDH specific siRNA transfected and PA-treated (G) were immunoprecipitated with antibodies against ACADS or ACADM, and succinylation level of these two proteins and its quantifications were shown.

(H) PA-treated H9C2 cells were transfected with siRNA for mGPDH and overexpressing plasmids for SIRT5_WT or catalytically inactive SIRT5-H158Y mutant, cell lysates were immunoprecipitated with antibodies against ACADS, and succinylation level of ACADS and its quantifications were assessed.

(I) PA-treated H9C2 cells were either untreated or treated with the proteasome inhibitors MG132 (MG), ACADS levels were analyzed by western blot and its quantifications were shown.

(J) PA-treated H9C2 cells were transfected with siRNA for mGPDH, cell lysates were immunoprecipitated with antibodies against ACADS, and ubiquitinated ACADS levels were assessed.

(K–M) PA-treated H9C2 cells were transfected with siRNA for mGPDH and overexpressing plasmids for HA-tagged ACADS_WT, ACADS-K250R and ACADS-K250E, succinylation level of ACADS (K), ACADS protein (L) and ubiquitination of ACADS (M) were assessed. Quantifications of K and L were shown. $n = 3$ mice per group for B-E, $n = 6$ mice per group for F, $n = 3$ per group for G-M. The data are presented as the means ± S.E.M. ***$p < 0.001$ by two-tailed unpaired Student's t test.

obesity-induced cardiac hypertrophy, fibrosis, and lipid accumulation (Figures 6C–6E). Similar therapeutic effects were observed in ob/ob mice injected with AA9-cTnT-mGPDH (Figures 6F–6J). Moreover, mGPDH overexpression elevated FAO rate (both *in vitro* and *ex vivo*) and FAs-driven energy generation (Figures 6K, 6L, and S11B), implying the reinforced mitochondrial function and energy production in hearts after mGPDH treatment, which was consistent with our mechanistic explorations. Together, these findings indicated that rescuing mGPDH expression significantly improve cardiac function, and might be a potential therapeutic avenue to combat lipotoxic cardiomyopathy in the context of obesity and diabetes.

DISCUSSION

Lipotoxic cardiomyopathy characterized by excessive myocardial lipid accumulation, has become an emerging cause of heart dysfunction in patients with obese and type 2 diabetic. However, currently, its pathological mechanisms remain unclear and treatment options are still limited. In the present study, we demonstrated that deficiency of mGPDH caused myocardial lipid accumulation and promoted the progression of HFD-induced lipotoxic cardiomyopathy. Multiple lines of evidences support our conclusion: (i) myocardial mGPDH expression were reduced in obese and diabetic mice and patients; (ii) HFD-induced lipotoxic cardiomyopathy mice with the cardiac deletion of mGPDH showed deteriorated cardiac structural and functional disorders, myocardial lipid accumulation and attenuated FAO; (iii) the downregulated SIRT5 expression in mGPDH deleted mice contributed to the lysine hypersuccinylation of FAO enzymes, such as ACADS, by promoting its degradation; (iv) cardiac-specific overexpression of SIRT5 in obese mGPDH cKO mice abrogated the aforementioned effects induced by mGPDH deficiency; (v) rescuing the insufficiency of mGPDH in myocardium of obese mice retarded the progression of lipotoxic cardiomyopathy.

Several pathophysiology for obesity/diabetes-related lipotoxic cardiomyopathy has been proposed by previous studies, such as the impaired energy metabolism, excessive generation of reactive oxygen species (ROS) and reactive nitrogen species, and disrupted Ca^{2+} cycling.[37–40] Notably, all these alterations are associated with mitochondrial dysfunction. As a mitochondrial inner membrane protein, current observations uncovered a crucial role of mGPDH deficiency in promoting mitochondrial dysfunction and cardiomyopathy during lipid and glucose metabolic disorders. The pathological insights into a correlation between decreased mGPDH and obesity/diabetes-related cardiomyopathy were functionally validated by cardiac mGPDH ablation *in vivo* and *in vitro*. Importantly, lipid accumulation and the impairment of cardiac function induced by mGPDH inhibition were clearly observed under HFD condition but not NCD, suggested that mGPDH deficiency could potentially be a genetic background factor that exacerbates the development of diet-induced cardiomyopathy, which is similar to our previous report of identifying the role of mGPDH in hepatic steatosis.[10]

The expression of mGPDH is widespread in the body and its functions are diverse. Including our group, previous studies revealed that mGPDH could regulate skeletal muscle regeneration via AMPK/mitochondrial biogenesis pathway;[28] liver-specific deletion mGPDH exacerbated diet-induced TG accumulation and steatosis through mediating calcium efflux between mitochondrial and ER;[10] kidney-specific deletion mGPDH exacerbated diabetes- or adriamycin-induced renal injury via S100/RAGE pathway modulated mitochondrial bioenergetics and ROS generation;[9] macrophage mGPDH regulated bacterial lipopolysaccharide induced inflammatory responses through modulating histone acetylation at genes encoding inflammatory mediators.[41] These findings highlighted the effects of mGPDH on multiple mitochondrial functions during different pathological and physiological processes.

In addition, our study demonstrated that lysine desuccinylase SIRT5 mediated mGPDH deletion induced cardiac lipotoxicity and dysfunction under HFD conditions. SIRT5 was known for regulating metabolic pathways, such as its participation in promoting urea cycle function[42] and purine metabolism.[43] After it was identified as a robust desuccinylase, hundreds of proteins were screened as potential desuccinylation substrates of SIRT5 by recent proteomic analyses,[27,30,35] and additional metabolic regulation functions of SIRT5 have been revealed. For

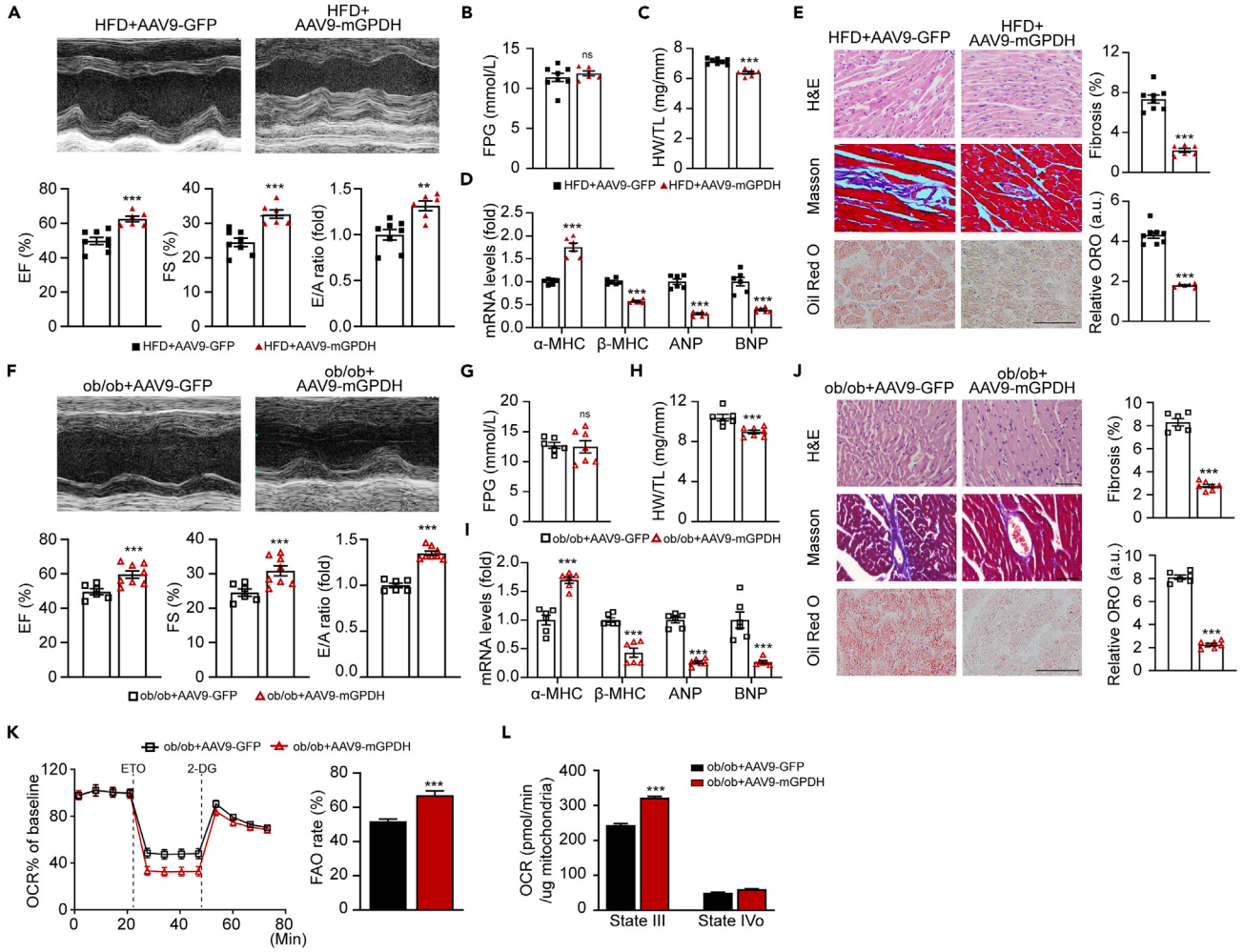

Figure 6. Rescuing mGPDH prevents obesity induced myocardial lipid accumulation and cardiomyopathy in HFD-fed and ob/ob mice

(A–E) HFD-fed mice were infected with AAV9-cTnT-GFP or AAV9-cTnT-mGPDH. Representative echocardiographic images of LV M-Mode traces were shown, and LV EF, FS, and E/A ratio were calculated (A). Fasting glucose (B), HW/TL(C), and mRNA expression of the hypertrophic gene (D) were assessed. H&E, Masson's Trichrome, and Oil red O staining in indicated group, and quantifications of fibrosis and lipid accumulation were shown (E).

(F–J) ob/ob mice were infected with AAV9-cTnT-GFP or AAV9-cTnT-mGPDH. Representative echocardiographic images of LV M-Mode traces were shown, and LV EF, FS, and E/A ratio were calculated (F). Fasting glucose (G), HW/TL (H), and mRNA expression of the hypertrophic gene (I) were assessed. H&E, Masson's Trichrome, and Oil red O staining in indicated group, and quantifications of fibrosis and lipid accumulation were shown (J).

(K) FAO of cardiomyocytes isolated from indicated group were evaluated by etomoxir (ETO)-inhibitable OCR method.

(L) Mitochondria were isolated from indicated mice, and mitochondrial energetics were evaluated by palmitoyl-*l*-carnitine/malate driven respiration measured by Seahorse analyzer. State III (+ADP) and state IVo (+oligomycin). Scale bar, 50 μm for E and J. n = 6–8 mice per group for A-J, *n* = 3 mice per group for K and L. The data are presented as the means ± S.E.M. $^{**}p < 0.01$, $^{***}p < 0.001$, ns, not significant by two-tailed unpaired Student's t test.

instance, knocked out SIRT5 increased the succinylation of the mitochondrial uncoupling protein 1 (UCP1) and resulted in brown adipose tissue dysfunction.[44] Our study suggested SIRT5 as an upstream regulator for FA enzymes in the context of HFD circumstance, and lysine desuccinylase might be the key mechanism under this regulation. Notably, despite we identified SIRT5 as the major mediator of mGPDH regulated cardiac FA metabolism, we cannot rule out the possibility that other proteins which are solely succinylated by mGPDH may also be involved in this process.

Interesting, both our results in Figure 3E and F and previous findings[45,46] suggested increased FAO rate in obese and diabetic hearts when compared with healthy controls. Therefore, some researchers considered this increasing cardiac FAO as a culprit in the development of obesity/diabetes-induced cardiomyopathy,[45,46] and decreased FAO may be beneficial for cardiomyopathy.[47] Actually, the role of FAO in obesity/diabetes-induced cardiomyopathy is always been controversial, many other researches have shown that decreased FAO may be harmful for cardiomyopathy.[48–50] Therefore, based on existing experimental evidences, the role of FAO in cardiomyopathy is complex, and cannot be simply described as beneficial or harmful. For example, Dan Shao et al.[14] increased FAO in heart by the deletion of acetyl

coenzyme A carboxylase 2 (ACC2), a well-established FAO regulator, and revealed that a rise in FAO alleviated the cardiovascular phenotype including systolic dysfunction, diastolic dysfunction, and fibrosis. Thus, they concluded that an increase in cardiac FAO protects against cardiomyopathy in chronically obese mice. Ours finding agreed with this observation and others aforementioned reports[48–50] by showing that the inhibition of mGPDH suppressed FAO in the heart and exacerbated cardiac dysfunction in HFD-induced mice. Moreover, we also assessed FAO in different HFD feeding periods, and observed an augmented FAO in mice fed with HFD for 8 weeks as compared with NCD. Although this increase of FAO was sustained statistically significant in mice fed with 12- and 24-week HFD, the obtained FAO at both time points were markedly decreased when compared with 8 weeks HFD feeding (data were not shown), and this decrease trend was in accordance with the reduced mGPDH expression in the hearts from mice with obesity and diabetes. Therefore, the effects of FAO in cardiomyopathy are likely to vary depending on diverse circumstance, and thereby shown to be beneficial in some cases and harmful in others.

In addition, the purpose of this study is not primarily aimed to figure out whether FAO is beneficial or harmful for cardiomyopathy, but to observe the role and mechanism of mGPDH in cardiomyopathy. During the experimental process, we discovered that deficient of mGPDH can exacerbate HFD-induced cardiomyopathy through repressing FAO. In this case, mGPDH deficiency induced the downregulation of FAO is harmful to cardiomyopathy, but this downregulation of FAO is not an initiating factor and is driven by mGPDH deficiency. Thus, our study has added evidence for the functionality of FAO under specific conditions, i.e., mGPDH deficiency. This is profitable for a more specific and more comprehensive understanding of the effect of FAO in cardiomyopathy, not merely benefit or harmful.

As for the modeling methods, in current study, we fed mice with 24 weeks HFD, and observed significant changes in systolic dysfunction, diastolic dysfunction, and fibrosis, which consistent with previous studies.[14,16,51–53] Base on the significant changes of the cardiac phenotypes, the model used in this study can guarantee the experimental observations and the conclusion drawing, which is also consistent with the researches we listed above. Indeed, some studies reported that HFD was not successful in modeling cardiac dysfunction. Although some researchers thought that it may be related to the duration of HFD feeding,[15,54,55] the reason for the inconsistency between different studies is not completely clear, and worth to be explored in the future.

In summary, we reveal that mGPDH is a central regulator of cardiac lipid accumulation and function in obesity and diabetes induced lipotoxic cardiomyopathy. Its deficiency down-regulated mitochondrial lipid oxidation through the SIRT5-mediated posttranslational modification of FAO enzymes. While over-expressing mGPDH in obese mice improved characteristics of lipotoxic cardiomyopathy, i.e., cardiac lipid accumulation, dysfunctions, hypertrophy and fibrosis, this represents a promising therapeutic intervention for this disease.

Limitations of the study

This study has some limitations. Mouse cardiac diastolic functions were assessed by tissue Doppler echocardiography in the current study, while the fast heart rate is a challenge for this noninvasive test. Thus, for subtle changes, invasive hemodynamic evaluation is usually considered as the gold standard for this kind of testing.

STAR★METHODS

Detailed methods are provided in the online version of this paper and include the following:

- KEY RESOURCES TABLE
- RESOURCE AVAILABILITY
  - Lead contact
  - Materials availability
  - Data and code availability
- EXPERIMENTAL MODEL AND STUDY PARTICIPANT DETAILS
  - Human material
  - Animals
- METHOD DETAILS
  - Human samples
  - Animal study
  - Cell isolation and culture
  - Echocardiography
  - Histology
  - Ultra-performance liquid chromatography (UPLC) and mass spectrometry (MS/MS) analysis
  - Stable isotope-labeled nutrient-uptake and -oxidation analysis
  - Mouse heart mitochondria isolation
  - Seahorse metabolic assay
  - Real-time reverse transcription polymerase chain reaction (qRT-PCR)
  - Western blot and immunoprecipitation
  - Identification and quantitation of lysine-succinylated peptides
- QUANTIFICATION AND STATISTICAL ANALYSIS

SUPPLEMENTAL INFORMATION

Supplemental information can be found online at https://doi.org/10.1016/j.isci.2024.109796.

ACKNOWLEDGMENTS

This work was supported by the National Science Fund for Distinguished Young Scholars (No. 81925007) and Excellent Young Scholars (82122013), the National Natural Science Foundation of China (No. 82230025, No. 82070836, No. 82070881, No. 81970752, No. 82000769 and No. 82100910), the Chongqing Distinguished Young Scholars (CSTB2022NSCQ-JQX0002), and the "Talent Project" of Army Medical University (2019R012, 2019R047 and 2019XQYYYJ003-2). BioRender was used to generate schematic figures.

AUTHOR CONTRIBUTIONS

H.Q., Y.Z., XF.L., QS.H., and NX.H.: designed and conducted *in vivo* and *in vitro* experiments, acquisition of data, and performed statistical analysis; H.Q., XF.L., LL.Z., YR.W., X.X., JB.L., C.W., and XL.G.: analysis and interpretation of data; JR.Z. and HL.Y. performed animal studies and helped with data analysis; Y.Z., and H.Q.: drafting of the article; QW.Y, G.L, GY.Y, ZM.Z, HT.Z., and Y.Z.: critical revision of the article for important intellectual content; HT.Z., Y.Z., and H.Q.: the guarantor of this work and, as such, had full access to all the data in the study and took responsibility for the integrity of the data and the accuracy of the data analysis.

DECLARATION OF INTERESTS

The authors declare no competing interests.

Received: June 13, 2023
Revised: March 21, 2024
Accepted: April 18, 2024
Published: May 11, 2024

REFERENCES

1. Yang, J., Sambandam, N., Han, X., Gross, R.W., Courtois, M., Kovacs, A., Febbraio, M., Finck, B.N., and Kelly, D.P. (2007). CD36 deficiency rescues lipotoxic cardiomyopathy. Circ. Res. *100*, 1208–1217. https://doi.org/10.1161/01.RES.0000264104.25265.b6.
2. Nakamura, M., Liu, T., Husain, S., Zhai, P., Warren, J.S., Hsu, C.P., Matsuda, T., Phiel, C.J., Cox, J.E., Tian, B., et al. (2019). Glycogen Synthase Kinase-3α Promotes Fatty Acid Uptake and Lipotoxic Cardiomyopathy. Cell Metab. *29*, 1119–1134.e12. https://doi.org/10.1016/j.cmet.2019.01.005.
3. van de Weijer, T., Schrauwen-Hinderling, V.B., and Schrauwen, P. (2011). Lipotoxicity in type 2 diabetic cardiomyopathy. Cardiovasc. Res. *92*, 10–18. https://doi.org/10.1093/cvr/cvr212.
4. Lee, W.S., and Kim, J. (2017). Diabetic cardiomyopathy: where we are and where we are going. Korean J. Intern. Med. *32*, 404–421. https://doi.org/10.3904/kjim.2016.208.
5. Palomer, X., Aguilar-Recarte, D., García, R., Nistal, J.F., and Vázquez-Carrera, M. (2021). Sirtuins: To Be or Not To Be in Diabetic Cardiomyopathy. Trends Mol. Med. *27*, 554–571. https://doi.org/10.1016/j.molmed.2021.03.004.
6. Sun, Y., Zhou, S., Guo, H., Zhang, J., Ma, T., Zheng, Y., Zhang, Z., and Cai, L. (2020). Protective effects of sulforaphane on type 2 diabetes-induced cardiomyopathy via AMPK-mediated activation of lipid metabolic pathways and NRF2 function. Metabolism *102*, 154002. https://doi.org/10.1016/j.metabol.2019.154002.
7. Tsushima, K., Bugger, H., Wende, A.R., Soto, J., Jenson, G.A., Tor, A.R., McGlauflin, R., Kenny, H.C., Zhang, Y., Souvenir, R., et al. (2018). Mitochondrial Reactive Oxygen Species in Lipotoxic Hearts Induce Post-Translational Modifications of AKAP121, DRP1, and OPA1 That Promote Mitochondrial Fission. Circ. Res. *122*, 58–73. https://doi.org/10.1161/CIRCRESAHA.117.311307.
8. Eto, K., Tsubamoto, Y., Terauchi, Y., Sugiyama, T., Kishimoto, T., Takahashi, N., Yamauchi, N., Kubota, N., Murayama, S., Aizawa, T., et al. (1999). Role of NADH shuttle system in glucose-induced activation of mitochondrial metabolism and insulin secretion. Science *283*, 981–985. https://doi.org/10.1126/science.283.5404.981.
9. Qu, H., Gong, X., Liu, X., Zhang, R., Wang, Y., Huang, B., Zhang, L., Zheng, H., and Zheng, Y. (2021). Deficiency of Mitochondrial Glycerol 3-Phosphate Dehydrogenase Exacerbates Podocyte Injury and the Progression of Diabetic Kidney Disease. Diabetes *70*, 1372–1387. https://doi.org/10.2337/db20-1157.
10. Zheng, Y., Qu, H., Xiong, X., Wang, Y., Liu, X., Zhang, L., Liao, X., Liao, Q., Sun, Z., Ouyang, Q., et al. (2019). Deficiency of Mitochondrial Glycerol 3-Phosphate Dehydrogenase Contributes to Hepatic Steatosis. Hepatology *70*, 84–97. https://doi.org/10.1002/hep.30507.
11. Madiraju, A.K., Erion, D.M., Rahimi, Y., Zhang, X.M., Braddock, D.T., Albright, R.A., Prigaro, B.J., Wood, J.L., Bhanot, S., MacDonald, M.J., et al. (2014). Metformin suppresses gluconeogenesis by inhibiting mitochondrial glycerophosphate dehydrogenase. Nature *510*, 542–546. https://doi.org/10.1038/nature13270.
12. Werfel, S., Jungmann, A., Lehmann, L., Ksienzyk, J., Bekeredjian, R., Kaya, Z., Leuchs, B., Nordheim, A., Backs, J., Engelhardt, S., et al. (2014). Rapid and highly efficient inducible cardiac gene knockout in adult mice using AAV-mediated expression of Cre recombinase. Cardiovasc. Res. *104*, 15–23. https://doi.org/10.1093/cvr/cvu174.
13. Yue, Z., Chen, J., Lian, H., Pei, J., Li, Y., Chen, X., Song, S., Xia, J., Zhou, B., Feng, J., et al. (2019). PDGFR-β Signaling Regulates Cardiomyocyte Proliferation and Myocardial Regeneration. Cell Rep. *28*, 966–978.e4. https://doi.org/10.1016/j.celrep.2019.06.065.
14. Shao, D., Kolwicz, S.C., Jr., Wang, P., Roe, N.D., Villet, O., Nishi, K., Hsu, Y.W.A., Flint, G.V., Caudal, A., Wang, W., et al. (2020). Increasing Fatty Acid Oxidation Prevents High-Fat Diet-Induced Cardiomyopathy Through Regulating Parkin-Mediated Mitophagy. Circulation *142*, 983–997. https://doi.org/10.1161/circulationaha.119.043319.
15. Li, H., Fan, J., Zhao, Y., Zhang, X., Dai, B., Zhan, J., Yin, Z., Nie, X., Fu, X.D., Chen, C., and Wang, D.W. (2019). Nuclear miR-320 Mediates Diabetes-Induced Cardiac Dysfunction by Activating Transcription of Fatty Acid Metabolic Genes to Cause Lipotoxicity in the Heart. Circ. Res. *125*, 1106–1120. https://doi.org/10.1161/CIRCRESAHA.119.314898.
16. Costantino, S., Akhmedov, A., Melina, G., Mohammed, S.A., Othman, A., Ambrosini, S., Wijnen, W.J., Sada, L., Ciavarella, G.M., Liberale, L., et al. (2019). Obesity-induced activation of JunD promotes myocardial lipid accumulation and metabolic cardiomyopathy. Eur. Heart J. *40*, 997–1008. https://doi.org/10.1093/eurheartj/ehy903.
17. Walls, S.M., Cammarato, A., Chatfield, D.A., Ocorr, K., Harris, G.L., and Bodmer, R. (2018). Ceramide-Protein Interactions Modulate Ceramide-Associated Lipotoxic Cardiomyopathy. Cell Rep. *22*, 2702–2715. https://doi.org/10.1016/j.celrep.2018.02.034.

18. Schulze, P.C., Drosatos, K., and Goldberg, I.J. (2016). Lipid Use and Misuse by the Heart. Circ. Res. *118*, 1736–1751. https://doi.org/10.1161/CIRCRESAHA.116.306842.
19. Goldberg, I.J., Reue, K., Abumrad, N.A., Bickel, P.E., Cohen, S., Fisher, E.A., Galis, Z.S., Granneman, J.G., Lewandowski, E.D., Murphy, R., et al. (2018). Deciphering the Role of Lipid Droplets in Cardiovascular Disease: A Report From the 2017 National Heart, Lung, and Blood Institute Workshop. Circulation *138*, 305–315. https://doi.org/10.1161/CIRCULATIONAHA.118.033704.
20. Lopaschuk, G.D., Karwi, Q.G., Tian, R., Wende, A.R., and Abel, E.D. (2021). Cardiac Energy Metabolism in Heart Failure. Circ. Res. *128*, 1487–1513. https://doi.org/10.1161/CIRCRESAHA.121.318241.
21. Ren, J., Wu, N.N., Wang, S., Sowers, J.R., and Zhang, Y. (2021). Obesity cardiomyopathy: evidence, mechanisms, and therapeutic implications. Physiol. Rev. *101*, 1745–1807. https://doi.org/10.1152/physrev.00030.2020.
22. Kolwicz, S.C., Jr., Olson, D.P., Marney, L.C., Garcia-Menendez, L., Synovec, R.E., and Tian, R. (2012). Cardiac-specific deletion of acetyl CoA carboxylase 2 prevents metabolic remodeling during pressure-overload hypertrophy. Circ. Res. *111*, 728–738. https://doi.org/10.1161/CIRCRESAHA.112.268128.
23. Ritterhoff, J., Young, S., Villet, O., Shao, D., Neto, F.C., Bettcher, L.F., Hsu, Y.W.A., Kolwicz, S.C., Jr., Raftery, D., and Tian, R. (2020). Metabolic Remodeling Promotes Cardiac Hypertrophy by Directing Glucose to Aspartate Biosynthesis. Circ. Res. *126*, 182–196. https://doi.org/10.1161/CIRCRESAHA.119.315483.
24. Kim, C., Wong, J., Wen, J., Wang, S., Wang, C., Spiering, S., Kan, N.G., Forcales, S., Puri, P.L., Leone, T.C., et al. (2013). Studying arrhythmogenic right ventricular dysplasia with patient-specific iPSCs. Nature *494*, 105–110. https://doi.org/10.1038/nature11799.
25. Montaigne, D., Butruille, L., and Staels, B. (2021). PPAR control of metabolism and cardiovascular functions. Nat. Rev. Cardiol. *18*, 809–823. https://doi.org/10.1038/s41569-021-00569-6.
26. Sack, M.N. (2011). Emerging characterization of the role of SIRT3-mediated mitochondrial protein deacetylation in the heart. Am. J. Physiol. Heart Circ. Physiol. *301*, H2191–H2197. https://doi.org/10.1152/ajpheart.00199.2011.
27. Sadhukhan, S., Liu, X., Ryu, D., Nelson, O.D., Stupinski, J.A., Li, Z., Chen, W., Zhang, S., Weiss, R.S., Locasale, J.W., et al. (2016). Metabolomics-assisted proteomics identifies succinylation and SIRT5 as important regulators of cardiac function. Proc. Natl. Acad. Sci. USA *113*, 4320–4325. https://doi.org/10.1073/pnas.1519858113.
28. Liu, X., Qu, H., Zheng, Y., Liao, Q., Zhang, L., Liao, X., Xiong, X., Wang, Y., Zhang, R., Wang, H., et al. (2018). Mitochondrial glycerol 3-phosphate dehydrogenase promotes skeletal muscle regeneration. EMBO Mol. Med. *10*, e9390. https://doi.org/10.15252/emmm.201809390.
29. Du, J., Zhou, Y., Su, X., Yu, J.J., Khan, S., Jiang, H., Kim, J., Woo, J., Kim, J.H., Choi, B.H., et al. (2011). Sirt5 is a NAD-dependent protein lysine demalonylase and desuccinylase. Science *334*, 806–809. https://doi.org/10.1126/science.1207861.
30. Rardin, M.J., He, W., Nishida, Y., Newman, J.C., Carrico, C., Danielson, S.R., Guo, A., Gut, P., Sahu, A.K., Li, B., et al. (2013). SIRT5 regulates the mitochondrial lysine succinylome and metabolic networks. Cell Metab. *18*, 920–933. https://doi.org/10.1016/j.cmet.2013.11.013.
31. Du, Y., Hu, H., Qu, S., Wang, J., Hua, C., Zhang, J., Wei, P., He, X., Hao, J., Liu, P., et al. (2018). SIRT5 deacylates metabolism-related proteins and attenuates hepatic steatosis in ob/ob mice. EBioMedicine *36*, 347–357. https://doi.org/10.1016/j.ebiom.2018.09.037.
32. Houten, S.M., Violante, S., Ventura, F.V., and Wanders, R.J.A. (2016). The Biochemistry and Physiology of Mitochondrial Fatty Acid β-Oxidation and Its Genetic Disorders. Annu. Rev. Physiol. *78*, 23–44. https://doi.org/10.1146/annurev-physiol-021115-105045.
33. Greene, K.S., Lukey, M.J., Wang, X., Blank, B., Druso, J.E., Lin, M.C.J., Stalnecker, C.A., Zhang, C., Negrón Abril, Y., Erickson, J.W., et al. (2019). SIRT5 stabilizes mitochondrial glutaminase and supports breast cancer tumorigenesis. Proc. Natl. Acad. Sci. USA *116*, 26625–26632. https://doi.org/10.1073/pnas.1911954116.
34. Liu, X., Zhu, C., Zha, H., Tang, J., Rong, F., Chen, X., Fan, S., Xu, C., Du, J., Zhu, J., et al. (2020). SIRT5 impairs aggregation and activation of the signaling adaptor MAVS through catalyzing lysine desuccinylation. EMBO J. *39*, e103285. https://doi.org/10.15252/embj.2019103285.
35. Park, J., Chen, Y., Tishkoff, D.X., Peng, C., Tan, M., Dai, L., Xie, Z., Zhang, Y., Zwaans, B.M.M., Skinner, M.E., et al. (2013). SIRT5-mediated lysine desuccinylation impacts diverse metabolic pathways. Mol. Cell *50*, 919–930. https://doi.org/10.1016/j.molcel.2013.06.001.
36. Polletta, L., Vernucci, E., Carnevale, I., Arcangeli, T., Rotili, D., Palmerio, S., Steegborn, C., Nowak, T., Schutkowski, M., Pellegrini, L., et al. (2015). SIRT5 regulation of ammonia-induced autophagy and mitophagy. Autophagy *11*, 253–270. https://doi.org/10.1080/15548627.2015.1009778.
37. Tan, Y., Zhang, Z., Zheng, C., Wintergerst, K.A., Keller, B.B., and Cai, L. (2020). Mechanisms of diabetic cardiomyopathy and potential therapeutic strategies: preclinical and clinical evidence. Nat. Rev. Cardiol. *17*, 585–607. https://doi.org/10.1038/s41569-020-0339-2.
38. Hölscher, M.E., Bode, C., and Bugger, H. (2016). Diabetic Cardiomyopathy: Does the Type of Diabetes Matter? Int. J. Mol. Sci. *17*, 2136. https://doi.org/10.3390/ijms17122136.
39. Kenny, H.C., and Abel, E.D. (2019). Heart Failure in Type 2 Diabetes Mellitus. Circ. Res. *124*, 121–141. https://doi.org/10.1161/circresaha.118.311371.
40. Al Kury, L., Smail, M., Qureshi, M.A., Sydorenko, V., Shmygol, A., Oz, M., Singh, J., and Howarth, F.C. (2018). Calcium Signaling in the Ventricular Myocardium of the Goto-Kakizaki Type 2 Diabetic Rat. J. Diabetes Res. *2018*, 2974304. https://doi.org/10.1155/2018/2974304.
41. Langston, P.K., Nambu, A., Jung, J., Shibata, M., Aksoylar, H.I., Lei, J., Xu, P., Doan, M.T., Jiang, H., MacArthur, M.R., et al. (2019). Glycerol phosphate shuttle enzyme GPD2 regulates macrophage inflammatory responses. Nat. Immunol. *20*, 1186–1195. https://doi.org/10.1038/s41590-019-0453-7.
42. Nakagawa, T., Lomb, D.J., Haigis, M.C., and Guarente, L. (2009). SIRT5 Deacetylates carbamoyl phosphate synthetase 1 and regulates the urea cycle. Cell *137*, 560–570. https://doi.org/10.1016/j.cell.2009.02.026.
43. Nakamura, Y., Ogura, M., Ogura, K., Tanaka, D., and Inagaki, N. (2012). SIRT5 deacetylates and activates urate oxidase in liver mitochondria of mice. FEBS Lett. *586*, 4076–4081. https://doi.org/10.1016/j.febslet.2012.10.009.
44. Wang, G., Meyer, J.G., Cai, W., Softic, S., Li, M.E., Verdin, E., Newgard, C., Schilling, B., and Kahn, C.R. (2019). Regulation of UCP1 and Mitochondrial Metabolism in Brown Adipose Tissue by Reversible Succinylation. Mol. Cell *74*, 844–857.e7. https://doi.org/10.1016/j.molcel.2019.03.021.
45. Mazumder, P.K., O'Neill, B.T., Roberts, M.W., Buchanan, J., Yun, U.J., Cooksey, R.C., Boudina, S., and Abel, E.D. (2004). Impaired cardiac efficiency and increased fatty acid oxidation in insulin-resistant ob/ob mouse hearts. Diabetes *53*, 2366–2374. https://doi.org/10.2337/diabetes.53.9.2366.
46. Zhou, Y.T., Grayburn, P., Karim, A., Shimabukuro, M., Higa, M., Baetens, D., Orci, L., and Unger, R.H. (2000). Lipotoxic heart disease in obese rats: implications for human obesity. Proc. Natl. Acad. Sci. USA *97*, 1784–1789. https://doi.org/10.1073/pnas.97.4.1784.
47. Tuunanen, H., Engblom, E., Naum, A., Någren, K., Scheinin, M., Hesse, B., Juhani Airaksinen, K.E., Nuutila, P., Iozzo, P., Ukkonen, H., et al. (2008). Trimetazidine, a metabolic modulator, has cardiac and extracardiac benefits in idiopathic dilated cardiomyopathy. Circulation *118*, 1250–1258. https://doi.org/10.1161/CIRCULATIONAHA.108.778019.
48. Cheng, L., Ding, G., Qin, Q., Huang, Y., Lewis, W., He, N., Evans, R.M., Schneider, M.D., Brako, F.A., Xiao, Y., et al. (2004). Cardiomyocyte-restricted peroxisome proliferator-activated receptor-delta deletion perturbs myocardial fatty acid oxidation and leads to cardiomyopathy. Nat. Med. *10*, 1245–1250. https://doi.org/10.1038/nm1116.
49. Yan, J., Young, M.E., Cui, L., Lopaschuk, G.D., Liao, R., and Tian, R. (2009). Increased glucose uptake and oxidation in mouse hearts prevent high fatty acid oxidation but cause cardiac dysfunction in diet-induced obesity. Circulation *119*, 2818–2828. https://doi.org/10.1161/CIRCULATIONAHA.108.832915.
50. Wu, D., Jian, C., Peng, Q., Hou, T., Wu, K., Shang, B., Zhao, M., Wang, Y., Zheng, W., Ma, Q., et al. (2020). Prohibitin 2 deficiency impairs cardiac fatty acid oxidation and causes heart failure. Cell Death Dis. *11*, 181. https://doi.org/10.1038/s41419-020-2374-7.
51. Tong, M., Saito, T., Zhai, P., Oka, S.I., Mizushima, W., Nakamura, M., Ikeda, S., Shirakabe, A., and Sadoshima, J. (2021). Alternative Mitophagy Protects the Heart Against Obesity-Associated Cardiomyopathy. Circ. Res. *129*, 1105–1121. https://doi.org/10.1161/CIRCRESAHA.121.319377.
52. Xu, H., Yu, W., Sun, M., Bi, Y., Wu, N.N., Zhou, Y., Yang, Q., Zhang, M., Ge, J., Zhang, Y., and Ren, J. (2023). Syntaxin17 contributes to obesity cardiomyopathy through promoting mitochondrial Ca(2+) overload in a Parkin-MCUb-dependent manner. Metabolism *143*, 155551. https://doi.org/10.1016/j.metabol.2023.155551.
53. Sun, X., Han, F., Lu, Q., Li, X., Ren, D., Zhang, J., Han, Y., Xiang, Y.K., and Li, J. (2020). Empagliflozin Ameliorates Obesity-Related Cardiac Dysfunction by Regulating Sestrin2-Mediated AMPK-mTOR Signaling and Redox

Homeostasis in High-Fat Diet-Induced Obese Mice. Diabetes *69*, 1292–1305. https://doi.org/10.2337/db19-0991.

54. Battiprolu, P.K., Hojayev, B., Jiang, N., Wang, Z.V., Luo, X., Iglewski, M., Shelton, J.M., Gerard, R.D., Rothermel, B.A., Gillette, T.G., et al. (2012). Metabolic stress-induced activation of FoxO1 triggers diabetic cardiomyopathy in mice. J. Clin. Invest. *122*, 1109–1118. https://doi.org/10.1172/JCI60329.
55. Noyan-Ashraf, M.H., Shikatani, E.A., Schuiki, I., Mukovozov, I., Wu, J., Li, R.K., Volchuk, A., Robinson, L.A., Billia, F., Drucker, D.J., and Husain, M. (2013). A glucagon-like peptide-1 analog reverses the molecular pathology and cardiac dysfunction of a mouse model of obesity. Circulation *127*, 74–85. https://doi.org/10.1161/CIRCULATIONAHA.112.091215.
56. World Health Organization (2000). The Asia-Pacific Perspective: Redefining Obesity and its Treatment.
57. Alberti, K.G., and Zimmet, P.Z. (1998). Definition, diagnosis and classification of diabetes mellitus and its complications. Part 1: diagnosis and classification of diabetes mellitus provisional report of a WHO consultation. Diabet. Med. *15*, 539–553. https://doi.org/10.1002/(sici)1096-9136(199807)15:7<539::aid-dia668>3.0.co;2-s.
58. Kyriazis, I.D., Hoffman, M., Gaignebet, L., Lucchese, A.M., Markopoulou, E., Palioura, D., Wang, C., Bannister, T.D., Christofidou-Solomidou, M., Oka, S.I., et al. (2021). KLF5 Is Induced by FOXO1 and Causes Oxidative Stress and Diabetic Cardiomyopathy. Circ. Res. *128*, 335–357. https://doi.org/10.1161/circresaha.120.316738.
59. Fu, Y., Sun, Y., Wang, M., Hou, Y., Huang, W., Zhou, D., Wang, Z., Yang, S., Tang, W., Zhen, J., et al. (2020). Elevation of JAML Promotes Diabetic Kidney Disease by Modulating Podocyte Lipid Metabolism. Cell Metab. *32*, 1052–1062.e8. https://doi.org/10.1016/j.cmet.2020.10.019.
60. Yao, C.H., Liu, G.Y., Wang, R., Moon, S.H., Gross, R.W., and Patti, G.J. (2018). Identifying off-target effects of etomoxir reveals that carnitine palmitoyltransferase I is essential for cancer cell proliferation independent of beta-oxidation. PLoS Biol. *16*, e2003782. https://doi.org/10.1371/journal.pbio.2003782.
61. Yao, C.H., Fowle-Grider, R., Mahieu, N.G., Liu, G.Y., Chen, Y.J., Wang, R., Singh, M., Potter, G.S., Gross, R.W., Schaefer, J., et al. (2016). Exogenous Fatty Acids Are the Preferred Source of Membrane Lipids in Proliferating Fibroblasts. Cell Chem. Biol. *23*, 483–493. https://doi.org/10.1016/j.chembiol.2016.03.007.
62. Qu, H., Miao, T., Wang, Y., Tan, L., Huang, B., Zhang, L., Liu, X., Long, M., Zhang, R., Liao, X., et al. (2021). Dedicator of Cytokinesis 5 Regulates Keratinocyte Function and Promotes Diabetic Wound Healing. Diabetes *70*, 1170–1184. https://doi.org/10.2337/db20-1008.
63. Huang, D.W., Sherman, B.T., and Lempicki, R.A. (2009). Systematic and integrative analysis of large gene lists using DAVID bioinformatics resources. Nat. Protoc. *4*, 44–57. https://doi.org/10.1038/nprot.2008.211.
64. Huang, D.W., Sherman, B.T., and Lempicki, R.A. (2009). Bioinformatics enrichment tools: paths toward the comprehensive functional analysis of large gene lists. Nucleic Acids Res. *37*, 1–13. https://doi.org/10.1093/nar/gkn923.

STAR★METHODS

KEY RESOURCES TABLE

REAGENT or RESOURCE	SOURCE	IDENTIFIER
Antibodies		
Mouse monoclonal anti-GPD2 Antibody (D-12)	Santa Cruz	Cat# sc-390830; RRID: AB_3068579
Rabbit polyclonal anti-GPD2 antibody (EPR14259)	Abcam	Cat# ab188585; RRID: AB_3068580
Mouse monoclonal anti-GPD1 Antibody (E-7)	Santa Cruz	Cat# sc-376219; RRID: AB_10989754
Rabbit polyclonal anti-ACADL antibody	Proteintech	Cat# 17526-1-AP; RRID: AB_2219661
Rabbit polyclonal anti-ACADM antibody	Proteintech	Cat# 55210-1-AP; RRID: AB_10837361
Rabbit polyclonal anti-ACADVL antibody	Proteintech	Cat# 14527-1-AP; RRID: AB_2288885
Rabbit polyclonal anti-ECHS1 antibody	Proteintech	Cat# 11305-1-AP; RRID: AB_2262166
Mouse monoclonal anti-SIRT1 antibody	Proteintech	Cat# 60303-1-Ig; RRID: AB_2881417
Rabbit polyclonal anti-SIRT2 antibody	Proteintech	Cat# 19655-1-AP; RRID: AB_2878592
Rabbit polyclonal anti-SIRT3 antibody	Proteintech	Cat# 10099-1-AP; RRID: AB_2239240
Mouse monoclonal anti-SIRT4 antibody	Proteintech	Cat# 66543-1-Ig; RRID: AB_2881905
Rabbit polyclonal anti-SIRT5 antibody	Proteintech	Cat# 15122-1-AP; RRID: AB_2188778
Rabbit polyclonal anti-SIRT6 antibody	Proteintech	Cat# 13572-1-AP; RRID: AB_2188915
Rabbit polyclonal anti-SIRT7 antibody	Affinity Biosciences	Cat# DF6161; RRID: AB_2838128
Rabbit polyclonal anti-Succinylysine antibody	PTM BIO	Cat# PTM-401; RRID: AB_2687628
Rabbit polyclonal anti-ACADS antibody	Proteintech	Cat# 16623-1-AP; RRID: AB_10666165
Rabbit monoclonal anti-ACADM Antibody (EPR3708)	Abcam	Cat# ab92461; RRID: AB_10563530
Rabbit monoclonal anti-HA Antibody (C29F4)	Cell Signaling Technology	Cat# #3724; RRID: AB_3068581
Bacterial and virus strains		
Adeno-associated virus 9-cardiac troponin T-Cre	Genomeditech	N/A
Adeno-associated virus 9-cardiac troponin T-GPD2	BioeGene	N/A
Adeno-associated virus 9-cardiac troponin T-SIRT5	BioeGene	N/A
Adeno-associated virus 9-shSIRT5	BioeGene	N/A
Biological samples		
Human heart samples	the Second Affiliated Hospital of Army Medical University	This paper
Chemicals, peptides, and recombinant proteins		
Rodent Diet with 60% kcal% fat	Research Diets	D12492
Streptozotocin	Sigma-Aldrich	S0130; CAS: 18883-66-4
Hanks' Balanced Salt Solution	Gibco	Cat#14025092
Fetal bovine serum	HyClone	Cat#sv30208
Penicillin-Streptomycin solution	Hyclone	Cat#SV30010
Collagenase II	Solarbi	Cat#C8150; CAS: 9001-12-1
Hyaluronidase	Solarbi	Cat#H8030; CAS: 37326-33-3
Dulbecco Modified Eagle Medium	Gibco	Cat#C11995500BT
Lipofectamine RNAiMAX Transfection Reagent	Invitrogen	Cat#13778150
Lipofectamine 3000 Reagent	Invitrogen	Cat#L3000075
^{13}C labeling palmitic acid	Sigma-Aldrich	Cat#292125; CAS: 57677-53-9
^{13}C labeling glucose	Sigma-Aldrich	Cat#389374; CAS: 110187-42-3

(*Continued on next page*)

Continued

REAGENT or RESOURCE	SOURCE	IDENTIFIER
XF assay medium	Seahorse	Cat#103576-100
Etomoxir	MCE	Cat#HY-50202A; CAS: 828934-41-4
2-deoxyglucose	MCE	Cat# HY-13966; CAS: 154-17-6
Critical commercial assays		
Primary Cardiomyocyte Isolation Kit	Thermo Fisher Scientific	Cat#88281
Modified Oil Red O Staining Kit	Beyotime	Cat#C0158M
Hematoxylin and Eosin Staining Kit	Beyotime	Cat#C0105M
BCA Protein Assay Kit	Beyotime	Cat#P0011
XFp Extracellular Flux Analyzer	Seahorse Bioscience	N/A
PrimeScript™ RT reagent Kit	Takara	Cat#RR037A
SYBR Premix Ex Taq II	Takara	Cat#RR820A
Dynabeads™ Protein G Immunoprecipitation Kit	Invitrogen	Cat#10007D
Experimental models: Cell lines		
Primary neonatal rat cardiomyocytes	This paper	N/A
H9C2	BLUEFBIO	BFN60804388
Experimental models: Organisms/strains		
Mouse: ob/ob: C57BL/6JGpt-Lep^{em1Cflox}/Gpt	GemPharmatech	Strain NO.T009981
Mouse: db/db: BKS-Lepr^{em2Cd479}/Gpt	GemPharmatech	Strain NO.T002407
Mouse: C57BL/6: C57BL/6JGpt	GemPharmatech	Strain NO.N000013
Mouse: mGPDH$^{fl/fl}$: C57BL/6JGpt-Gpd2^{em1Cflox}/Gpt	GemPharmatech	Strain NO.T008780
Oligonucleotides		
siRNA targeting GPD2	BioeGene	N/A
Primers for qRT-PCR, see Table S5	This paper	N/A
Recombinant DNA		
Plasmid: mGPDH, SIRT5, SIRT5_H158Y, ACADS, ACADS_K250R, ACADS_K250E and control vector	GenScript or SinoBiological	N/A
Software and algorithms		
Graphpad Prism 8	GraphPad Software	https://www.graphpad.com/scientific-software/prism/
Seahorse Wave Software	Agilent Technologies	https://www.agilent.com/en/product/cell-analysis/real-time-cell-metabolic-analysis/xf-software/seahorse-wave-desktop-software-740897

RESOURCE AVAILABILITY

Lead contact

Further information and requests for resources and reagents should be directed to and will be fulfilled or facilitated by the lead contact Hongting Zheng (fnf7703@hotmail.com).

Materials availability

This study did not generate new unique reagents.

Data and code availability

- Data: The data sources of this study are presented in the ''STAR Methods'' sections.
- Code: This paper does not report the original code.
- All data related to our conclusions in current study are presented in the main text and/or supplemental information. Additional data related to this article is available from the lead contact upon request.

EXPERIMENTAL MODEL AND STUDY PARTICIPANT DETAILS

Human material

Human samples of atrial appendage were collected from patients undergoing heart valve replacement. A total of 6 obesity, 6 diabetes, and 5 lean/non-diabetic subjects (7 males and 10 females) were enrolled in this study. All protocols were approved by the Ethics Committee of the Second Affiliated Hospital of Army Medical University (institutional review board-approved protocol no. 2016-056-01), and were consistent with the principles of the Declaration of Helsinki. Informed consent was obtained from each recruited participant. Clinical information such as gender, ages was extracted from their medical records, and provided in Table S1, while ancestry, race or ethnicity was not provided.

Animals

Male ob/ob, db/db, C57BL/6, db/m, mGPDH$^{fl/fl}$ and mGPDH$^{wt/wt}$ mice were purchased from GemPharmatech Co., Ltd, Jiangsu, China. All animal protocols in this study were approved by the Laboratory Animal Welfare and Ethics Committee of the Army Medical University (No. AMUWEC20181456). Mice were transitioned to a HFD between the ages of 5 and 8 weeks, with further details regarding the duration of HFD maintenance provided in the Method details section. All mice were maintained on a 12-hour light, 12-hour dark cycle at 20-22°C with free access to water and normal chow diet or HFD.

METHOD DETAILS

Human samples

Generally, human subjects were screened with coronary computed tomography angiography, electrocardiogram, echocardiogram, blood pressure, thyroid disease analysis, etc. Patients with coronary artery disease, hypertensive heart disease, dilated cardiomyopathy, restrictive cardiomyopathies, and hyperthyroid cardiomyopathy were excluded. Obesity was defined BMI $\geq$ 25 kg/m^2 according to the diagnostic criteria recommended by the Western Pacific Regional Office (WPRO) of the World Health Organization (WHO).[56] Diabetes was diagnosis according to WHO 1998 criteria.[57]

Animal study

AAV9 (adeno-associated virus 9)-cTnT (cardiac troponin T)-Cre was generated by Genomeditech, Shanghai, China. Cardiomyocyte-specific mGPDH ablation (cKO) was generated by injecting mGPDH$^{fl/fl}$ mice with AAV9-cTnT-Cre (2 x 10^{11} viral genomes per mouse) via tail vein. cKO and its controls were subjects to a high-fat diet (HFD, 60% kcal fat, Research Diets Inc., D12492) feeding for 24 weeks. Intraperitoneal streptozotocin (STZ, Sigma-Aldrich, 50 mg/kg for 5 consecutive days) injection was used to induced type 1 diabetic mouse models according to our previous study.[9] Blood glucose was detected 1-week post-injection, and mice with fasting blood glucose levels higher than 13.9 mmol/l (250 mg/dl) were considered diabetic. For SIRT5 overexpression, db/db mice or mGPDH cKO mice fed with HFD for 16 weeks were injected by AAV9-cTnT-SIRT5 via tail vein, and then mice were maintained for 8 weeks before being sacrificed. To rescue mGPDH expression, HFD fed and ob/ob obese mice were injected with AAV9-cTnT-mGPDH through tail vein 8 weeks before sacrificed. To knockdown SIRT5 in mGPDH rescued obese mice, HFD mice were injected with AAV9-cTnT-mGPDH and AAV9-shSIRT5 through tail vein, and then mice were sacrificed 8 weeks later. Only male mice were included in this study.

Cell isolation and culture

Primary neonatal rat cardiomyocytes and non-cardiomyocytes (major types are fibroblasts and endothelial cells) were isolated from ventricles of neonatal rats (postnatal day 1-3, rat strain Sprague Dawley) using a Primary Cardiomyocyte Isolation Kit (Thermo Fisher Scientific, 88281) with some modifications. In brief, freshly isolated ventricles were minced into 1 to 3 mm^3 pieces and washed twice by cold HBSS, and then were incubated with mixed Cardiomyocyte Isolation Enzyme solution in a 37°C incubator for 30 to 35 min. After that, the enzyme solution was removed and the cells were washed twice with cold Hanks' Balanced Salt Solution (HBSS). Centrifuge the cell suspension at 50 x g for 1 min, and carefully remove the supernatant containing non-cardiomyocytes (e.g., fibroblasts, endothelial cells) into a new tube. The collected primary cells were then pre-plated on 10 cm petri dishes and incubated for 90 min for further cardiomyocyte selection. Isolated cardiomyocytes were then resuspended and cultured in complete DMEM for Primary Cell Isolation with 10% fetal bovine serum (HyClone, sv30208), Penicillin-Streptomycin solution (Hyclone, SV30010) and Cardiomyocyte Growth Supplement to reduce non-cardiomyocytes contamination and maintain cardiomyocytes at a high purity during the culture period. The supernatant containing non-cardiomyocytes was centrifuged at 250 x g for 10 min, the supernatant was discarded and cells were resuspended and cultured in DMEM supplemented with 10% fetal bovine serum and Penicillin-Streptomycin solution. All these cells were maintained at 37°C with 5% CO_2, and were not tested for mycoplasma.

Adult cardiac myocytes were isolated according to the protocol reported previously[2] with some modifications. Briefly, hearts were perfused with EDTA buffer, and then digested by perfusing with oxygenated Krebs-Henseleit Buffer supplemented with collagenase II (Solarbio, 0.5mg/ml) and hyaluronidase (Solarbio, 0.5mg/ml) at 37°C. Cardiomyocytes and non-cardiomyocytes were separated by 4 sequential rounds of gravity settling. Cardiomyocytes were used for further studies.

Rat H9C2 cardiomyoblasts were purchased from National Collection of Authenticated Cell Cultures (Shanghai, China), cultured in Dulbecco Modified Eagle Medium (DMEM, Gibco, C11995500BT) with 10% fetal bovine serum (HyClone, sv30208) and maintained at 37°C with 5% CO_2.

For gene knockdown experiments in H9C2 cells, mGPDH-specific and corresponding negative-control siRNAs were purchased from Qiagen, and were transfected into cells by using Lipofectamine RNAiMAX Transfection Reagent (Invitrogen) according to the manufacturer's instructions. For gene overexpression in H9C2 cells, mGPDH, SIRT5, SIRT5_H158Y, ACADS, ACADS_K250R, ACADS_K250E and control vector plasmids were generated by GenScript or SinoBiological, plasmids were transfected by using Lipofectamine 3000 Reagent (Invitrogen) according to the manufacturer's instructions.

Echocardiography

The cardiac functions were assessed by transthoracic echocardiography using Vevo 2100 system (VisualSonics Inc) as previous described.[58] Briefly, mice were anesthetized with isoflurane and their chest hair was shaved. After placing mice on a heating table, two-dimensional images of left ventricular (LV) parasternal short-axis views were obtained in the M-mode at the papillary muscle level. To evaluate LV systolic function and structure, LV internal diameter (LVID) and LV posterior wall thickness were measured at the end of systole and diastole, and Left ventricle volume, ejection fractions and fractional shortening were calculated. Left ventricle volume (LV Vol, diastole/systole) = ((7.0 / (2.4 + LVID;d/s)) x LVID;d/s^3); LV ejection fraction = 100 x ((LV Vol;d – LV Vol;s) / LV Vol;d); LV fractional shortening = 100 x ((LVID;d – LVID;s) / LVID;d). Diastolic function was determined by the ratio of early (E-wave) and late (A-wave) LV diastolic filling velocities (E/A ratio) using transmitral inflow Doppler.

Histology

Haematoxylin and eosin (H&E), Masson's Trichrome and Oil Red O staining were performed according to our previous describes.[9,10] For H&E and Masson's Trichrome staining, hearts were harvest and fixed in 4% paraformaldehyde for 24 hours at room temperature, and then cut into 4-6 μm thick sections. For Oil Red O Staining, hearts were frozen with Tissue-Tek OCT compound (Sakura Finetek) and cut into 8-10 μm thick sections; cells were fixed in formaldehyde solution. These frozen heart tissue sections or fixed cells were subjected to Oil Red O Staining.

Ultra-performance liquid chromatography (UPLC) and mass spectrometry (MS/MS) analysis

Lipidomic analysis for hearts were conducted according to previous reported.[59] Samples were placed in liquid nitrogen for 2 min and stored at -80°C. Then samples were subjected to liquid extraction. UPLC-MS/MS was performed by Metware Biotechnology Co., Ltd (Wuhan, China).

Stable isotope-labeled nutrient-uptake and -oxidation analysis

For lipid uptake assessment, cardiomyocytes were incubated in fresh medium for 6 hours. Known concentrations of ^{13}C labeling palmitic acid or glucose were added in medium 3 hours before sampled. Standard substances were dissolved and diluted to a final concentration of 1 mmol/l (stock solution), and a series of calibration standard solutions were then prepared by stepwise dilution of this stock solution. For ^{13}C labeling Fatty acid oxidation (FAO) assessment *ex vivo*, isolated mouse hearts were perfused in Langendorff-mode at 37°C and a constant pressure. After equilibration, hearts were perfused with ^{13}C-labeled palmitic acid and then were frozen in liquid nitrogen for further assessment according to previously described.[14,22] In details, during FAO, ^{13}C labeling palmitic acid undergoes degradation to form $^{13}C_2$-acetyl-CoA. Subsequently, this acetyl-CoA combines with oxaloacetate in the tricarboxylic acid (TCA) cycle to generate $^{13}C_2$-citrate (the M+2 isotopologue). Heart tissues, which had been frozen, were extracted using perchloric acid and subsequently neutralized with potassium hydroxide. For Metabolite extraction, samples were added 1000μL of precooled MeOH/H2O (3/1, v/v, at -40°C) to the samples, followed by vortexing for 30 seconds. The samples underwent three freeze-thaw cycles in liquid nitrogen after being precooled in dry ice. Subsequently, they were vortexed for 30 seconds and sonicated for 15 minutes in an ice-water bath. After incubating at -40°C for one hour, the samples were centrifuged at 12000 rpm for 15 minutes at 4°C, and 800μL of supernatant was collected and dried by spinning. The dried extracts were reconstituted with 200μL of ultrapure water and filtered through a centrifuge tube filter. Finally, the samples were transferred to injection vials for HPIC-MS/MS analysis after centrifuging at 12000 rpm for 15 minutes at 4°C. A quality control (QC) sample was generated by pooling all the samples, and then used for further HPIC-QE-MS Analysis. For ^{13}C labeling FAO assessment *in vitro*, cardiomyocytes were incubated with ^{13}C labeling palmitic acid, after labeling for 24 hours, cells were extracted and analyzed as previously described.[23,60,61] In details, cells were treated with 1000μL MeOH/H2O (3/1, v/v, precooled at -40°C) and vortexed for 30s. Samples underwent repeated freeze-thaw cycles in liquid nitrogen after precooling in dry ice. They were then vortexed for 30s, sonicated for 15 min in an ice-water bath, and incubated at -40°C for one hour. Following centrifugation at 12000 rpm for 15 min at 4°C, 800μL supernatant was collected and dried by spinning. Dry extracts were reconstituted with 200μL ultrapure water, filtered, and transferred to injection vials for HPIC-MS/MS analysis after centrifugation at 12000 rpm for 15 min at 4°C. A quality control (QC) sample was generated by pooling all the samples. HPIC-QE-MS analysis was conducted. The nutrient-uptake and -oxidation detections were performed by Biotree and Bioegene (Shanghai, China) using UPLC-MRM-MS method.

Mouse heart mitochondria isolation

Mitochondria were isolated from mouse heart by using a tissue mitochondria isolation kit from Beyotime (Shanghai, China) according to manufacturer's instruction. In brief, hearts were rinsed with ice-cold PBS and cut into pieces. These tissues were incubated with cold trypsin solution for 15 min on ice. After centrifugation, supernatant was discarded and mitochondria isolation buffer containing 0.2% BSA and 0.5mg/ml trypsin inhibitor were added to neutralize the trypsin. Mitochondria were isolated by differential centrifugation, and concentrations were determined by BCA protein assay kit (Beyotime, Shanghai, China).

Seahorse metabolic assay

FAO was assessed in adult cardiomyocytes and H9C2 cells as described previously.[2] Cells were plated at the Seahorse assay plates with XF assay medium containing DMEM with 5.5 mM glucose and 0.5 mM carnitine according to installation and operation manual from Seahorse Bioscience. Etomoxir (ETO, 250 μM), a specific CPT-1 inhibitor, was injected to assess the rate of FAO, and then 2-deoxyglucose (2-DG, 50 mM), a blocker of glycolysis and pyruvate oxidation, was used to assess glucose utilization.

Palmitoyl-L-carnitine/Malate driven respiration was calculated from oxygen consumption rates (OCRs) using XFp Extracellular Flux Analyzer (Seahorse Bioscience). Isolated mitochondria were suspended in the mitochondrial assay buffer, and 2 μg mitochondria were loaded in the assay plate with Palmitoyl-L-carnitine (50 μM)/Malate (2mM) as substrates for coupling assays. After incubated the plates in a 37°C nonCO_2 incubator, ADP (4mM) and oligomycin (2.5 mg/ml) were sequentially injected into each well to assess state III and state IVo respiration, respectively.

Real-time reverse transcription polymerase chain reaction (qRT-PCR)

qRT-PCR was performed according to our previous reported. Total RNA was prepared from heart tissue and cells using TRIzol (TIANGEN). RNA quality was evaluated by 260/280 ratio using a NanoDrop2000 spectrophotometer (Thermo Scientific). cDNA was generated using the PrimeScript RT Reagent Kit (TaKaRa). Using SYBR Premix Ex Taq II (TaKaRa), real-time PCR was performed on an Applied Biosystems 7300 system (Life Technologies). Gene expression was calculated using the ΔCt method, and the primer sequences are listed in Table S5.

Western blot and immunoprecipitation

Western blot and immunoprecipitation were performed as our described previously.[62] For western blot, the following antibodies were used: mGPDH from Santa Cruz (California, USA) and Abcam (Cambridge, MA, USA); ACADL, ACADM, ACADVL, ECHS1, and SIRT1-6 from Proteintech (Wuhan, China); SIRT7 from Affinity (Jiangsu, China); Succinyllysine from PTM bio (Zhejiang, China). For immunoprecipitation, cell or tissue were lysed in immunoprecipitation lysis buffer (Roche), and then were immunoprecipitated with specific antibodies: ACADS from Proteintech (Wuhan, China), ACADM from Abcam (Cambridge, MA, USA) and HA from (Cell Signaling Tech, China); and the immunoprecipitates were subjected to western blot with indicated antibodies.

Identification and quantitation of lysine-succinylated peptides

Lysine-succinylated peptides were identified and quantified by PTM Biolabs according to previous reported.[27,35] Briefly, tryptic digested peptides were dissolved in IP buffer (100 mM NaCl, 1 mM EDTA, 50 mM Tris-HCl, 0.5% NP-40, pH 8.0), and the supernatant was incubated with anti-succinyllysine antibody conjugated agarose beads (PTM Bio) at 4°C overnight with gentle rotation. After incubation, the beads were washed four times with IP buffer, two times with deionization water. The bound peptides were eluted from the beads by washing three times with 0.1% trifluoroacetic acid, and then eluents were collected, vacuum freeze dried, and cleaned up with C18 ZipTips (Millipore Corp.) according to the manufacturer's instructions. The tryptic digests were dissolved in HPLC solvent A (containing 0.1% formic acid and 2% acetonitrile) and separated by NanoElute ultra-high performance liquid system. Peptides were then implanted into the capillary ion source for ionization, and then analyzed by timsTOF Pro mass spectrometry. Enrichment analysis for KEGG pathway (Kanehisa and Goto, 2000) were performed by using DAVID Bioinformatics Resources.[63,64]

QUANTIFICATION AND STATISTICAL ANALYSIS

The data are presented as the means ± S.E.M., unless otherwise stated. Statistical analyses were performed by using GraphPad Prism8 software (San Diego, CA, USA). For two group comparisons, standard Student *t* test was used. For comparisons more than 2 groups, 1-way or 2-way ANOVA followed by the Tukey post hoc test were adopted. *P* values < 0.05 were considered statistically significant.